国際化推進共同研究概要

No. 1

タイトル： Thermo-mechanical stress et crystalline quality of mc-silicon for PV application.

研究代表者：GALLIEN, Benjamin

所内世話人：柿本　浩一

実 施 期 間：2012年10月21日～10月27日、11月1日～11月4日
（10/28～10/31は私費にて別用務有り）

研究概要：　太陽電池用シリコン結晶の成長、冷却プロセスに関して、数値解析コードを用いた新規解析手法の提案を行った。特に、太陽電池の特性を作用する転位等の欠陥密度の低減を大規模数値解析により可能とする新規方法に関する討論等の打ち合わせを行った。今後も、継続的に共同研究を継続する。

International Joint Research Report for 2012

Subject field: Renewable Energy Dynamics

Subtheme: Thermo-mechanical stress et crystalline quality of mc-silicon for PV application

RIAN attendant: Professor Koichi KAKIMOTO

Representative person: Mr. B. Gallien

Crystalline quality of silicon ingot depends of many factors. The thermal stress during the solidification and the cooling of the ingot is one of them and lead to multiplication of dislocation, a linear defect in the crystal. These dislocations are place of electron/hole recombination and so high dislocation density decrease the photovoltaic efficiency. Consequently, it is important to understand why the dislocation appears and know their density in the ingot at the end of cooling.

A numerical model has been created on Comsol software with purpose to answer this issue. The input of the model is the temperature map .vs. time of the ingot along the solidification and the cooling. With this data, the software calculates the thermo-mechanical stresses, the dislocation density and the plastic strain which relaxes the elastic stress. This model is based on the Alexander and Haasen model.

To validate this model, Professor Koichi Kakimoto sent us the thermal data of the simulation of a furnace corresponding of the data use in one of his publication. Mohammed M'Hamdi from Sintef (Norway) does the same. After validations of the model, it is used to calculate dislocation density for a furnace develops at INES (France). This last simulation will be compared with experimental results by characterization of dislocation density in a silicon ingot.

With these 3 simulations, we hope to publish a paper based on the international collaboration of these 3 groups.

That's why we think it will be interesting to come to your laboratory to compare the working method, the simulation and to organize the collaboration and paper redaction.

国際化推進共同研究概要

No. 2

タイトル： Comparative study on calibrating sensors for ferry observations.

研究代表者：LIU, Cho-Teng

所内世話人：松野　健

実 施 期 間：2012年5月12日 ～ 5月16日

研究概要： 台湾海峡および対馬海峡を横断するフェリーによってモニタリングされている蛍光光度の値を比較するため、台湾海峡のモニタリングを行っている台湾大学のグループが対馬海峡を横断するフェリー（ニューかめりあ）に乗船して採水分析を行った。往復観測後、台湾大学のグループは持参した分析機器を用いて九州大学でサンプルを分析し、ニューかめりあに搭載しているセンサーの値との比較を行った。センサーと採水分析の結果はよい相関を示したが、絶対値には3倍程度の差があり、九州大学が名古屋大学との共同で実施したキャリブレーションの結果とも相違が見られ、今後の検討が必要であることが示された。

Report on the Joint Research of 2012

"Comparative study on calibrating sensors for ferry observations"

List of participants

National Taiwan University Team

Prof. Cho-Teng Liu

Ms. Wen-Huei Lee

Mr. Shiang-Chi Shie

Mr. Wen-Hua Her

Kyushu University Team

Prof. Takeshi Matsuno

Prof. Joji Ishizaka of Nagoya Univ.

Dr. Ken-ichi Fukudome

Mr. KeunJong Lee

Abstract

A joint effort to measure the quality of water that enters or exits East China Sea was carried out at both Tsushima Strait and Taiwan Strait. To assure that the data form these two straits are compatible, and comparative experiment was carried out over New Camellia Ferry between Hakata and Busan. The results shows that the Chl-a data from automatic monitoring system works reliably and the data agrees with bottled data and satellite data. But, sensors require routine calibration.

Survey from Hakata to Busan:

The ferry New Camellia left Hakata Harbor at 12:30 pm of May 13 towards Busan of Korea. Figure 1 shows the cruise track and the speed (km/h) of ferry from harbor to harbor. She cruises at 41-45 km/h.

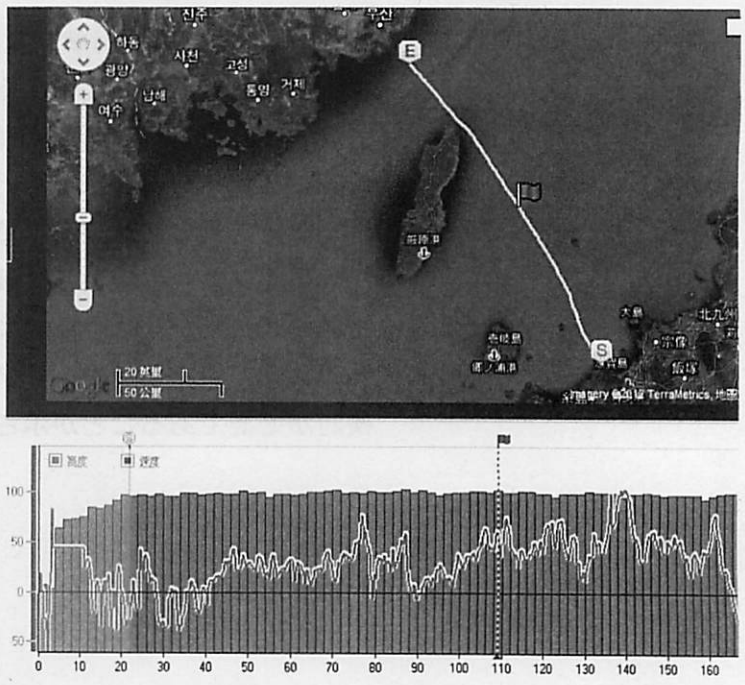

Fig 1: Cruise track and ship speed (km/h) of New Camellia from Hakata to Busan on May 13 of 2012.

At schedule time, the valve of bypass pipe was open to release the water in the pipe (Figure 2a), then 4 bottles of sea water were taken for Nagoya University and Taiwan University to filter (Figure 2b) and to analyze for Chl-a concentration.

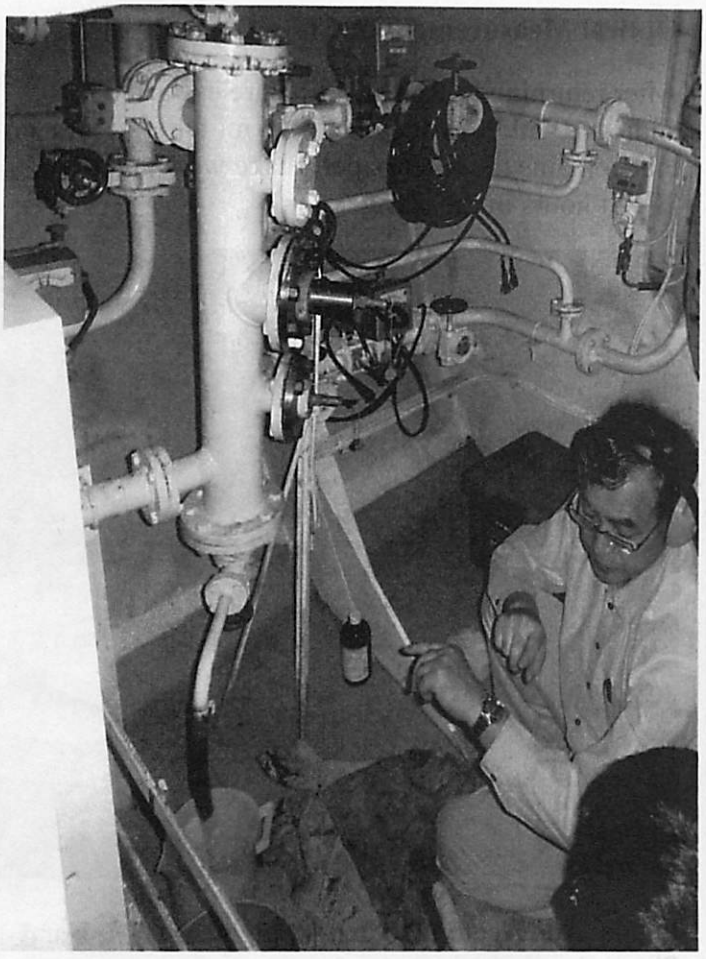

Fig 2a: Sampling sea water from bypass pipe on New Camellia.

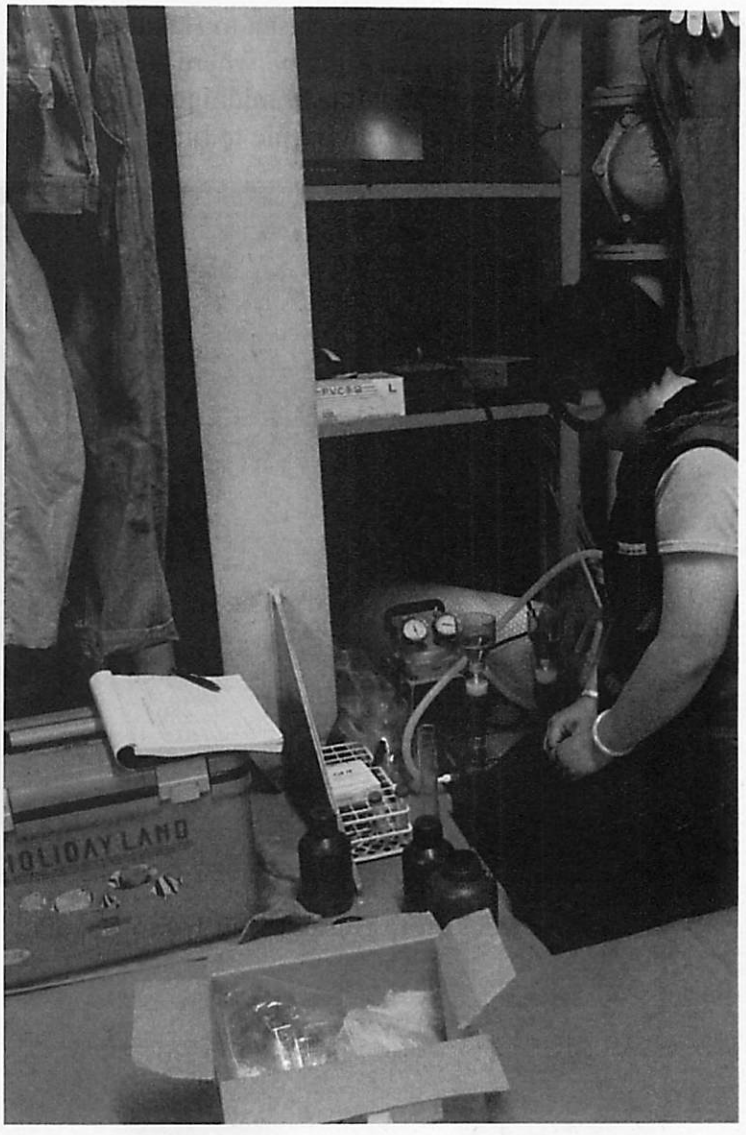

Fig 2b: Filtering water samples and store the filter paper in an ice chest that is kept freezing temperature with dry ice.

For the returning trip, from Busan to Hakata, the cruise track is shown in Figure 3 where New Camellia was near Tsushima at midnight (the color of ship track changes from purple to blue).

Fig 3: cruise track from Busan (May 14) to Hakata (May 15).

Optical Measurement of Chl-a concentration

After returning to RIAM, Chl-a are extracted by adding 10 ml 90% acetone to 15 ml tube (Figure 4a) that contains the filter paper, shake well, and store 20~24 hours in the refrigerator

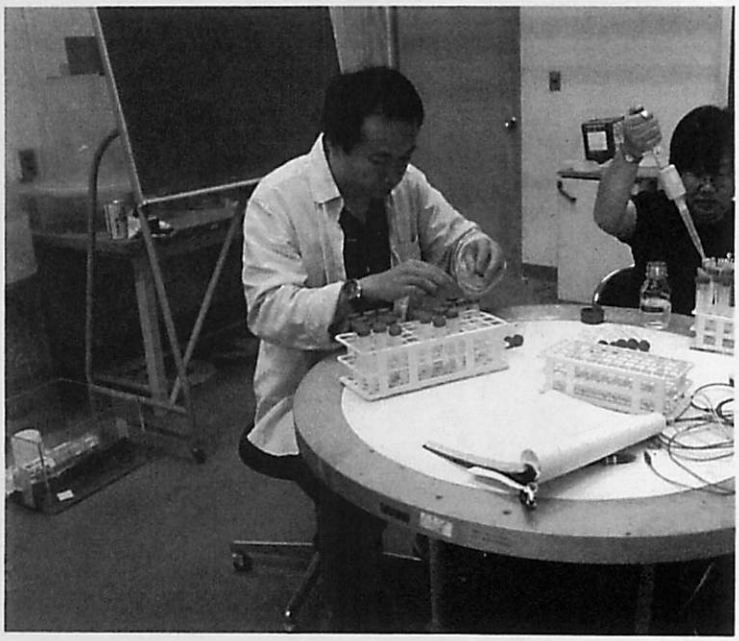

Fig 4a: Add Acetone to extract pigments (Chl-a and Phaeopigment).

On May 16, we centrifuged all tubes (Fig. 4b);
take 6 ml clear liquid,
measure the fluorescence with TURNER 10-AU Fluorometer (Fig. 4b)
add 200µl 1N HCl, shake well, re- measure the fluorescence
compute Chl-a and phaeopigment concentration

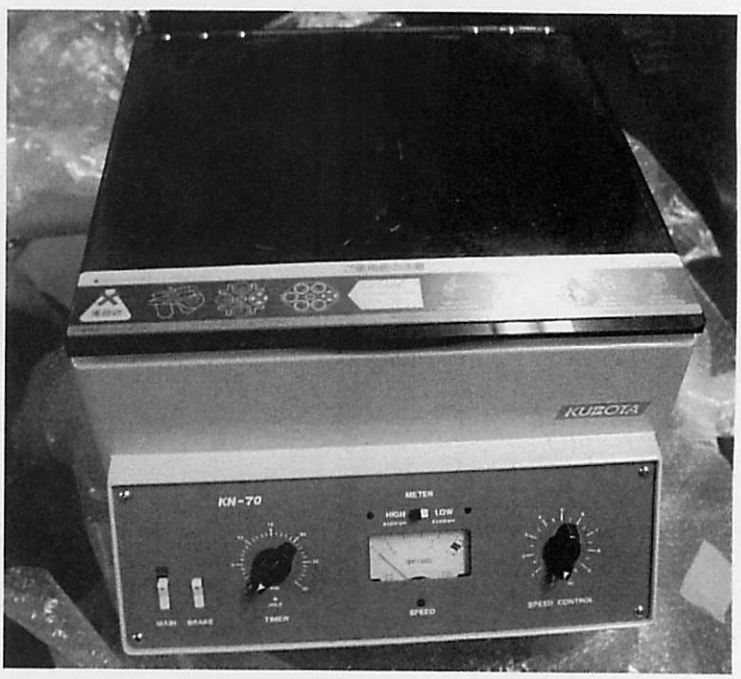

Fig. 4b: Centrifuge (top) and Fluorometer (bottom)

Data from sensor on the ferry and from chemical analysis

The Chl-a concentration (microgram/liter) from bottled data (from Nagoya University and from National Taiwan University) and the sensor data from New Camellia are listed in Table 1.

Table 1: Chlorophyll-a concentration (Chl-a) from sensor on the ferry, and from optical measurement by the group from Nagoya University and by the group from National Taiwan University.

day	Sample time (hhmm)	Chl-a, ferry	Chl-a, NU (ug/L)_Avg	Chl-a, N (ug/L)_A
2012/5/13	1420	0.24	0.317	0.122
2012/5/13	1500	0.235	0.215	0.131
2012/5/13	1530	0.244	0.376	0.146
2012/5/13	1600	0.467	0.512	0.171
2012/5/13	1630	0.395	0.291	0.150
2012/5/13	1700	0.403	0.215	0.113
2012/5/14	2312	0.874	0.534	0.229
2012/5/14	2332	0.34	0.162	0.071
2012/5/14	2351	0.238	0.084	0.053
2012/5/15	0010	0.299	0.118	0.055
2012/5/15	0030	0.404	0.126	0.078
2012/5/15	0050	1	0.723	0.307
2012/5/15	0110	0.89	0.603	0.283
2012/5/15	0130	0.506	0.276	0.118
2012/5/15	0150	0.389	0.248	0.093
2012/5/15	0210	0.738	0.632	0.257
2012/5/15	0230	0.775	0.549	0.184
2012/5/15	0250	1.03	0.696	0.289
2012/5/15	0310	0.997	0.673	0.264
2012/5/15	0330	0.326	0.223	0.075
2012/5/15	0350	0.883	0.534	0.208

The scatter plots of ferry data vs. NTU data of Chl-a are shown in Figure 5 for daytime, and Figure 6 for nighttime.

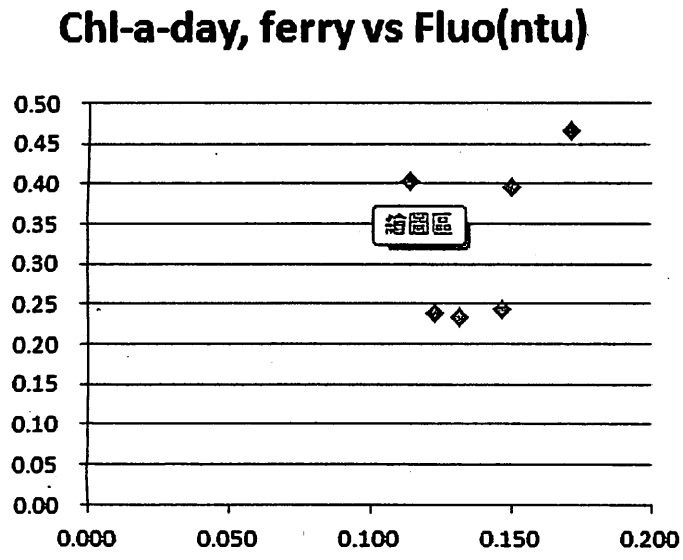

Fig 5: Daytime Chl-a data from ferry and from NTU's bottled water.

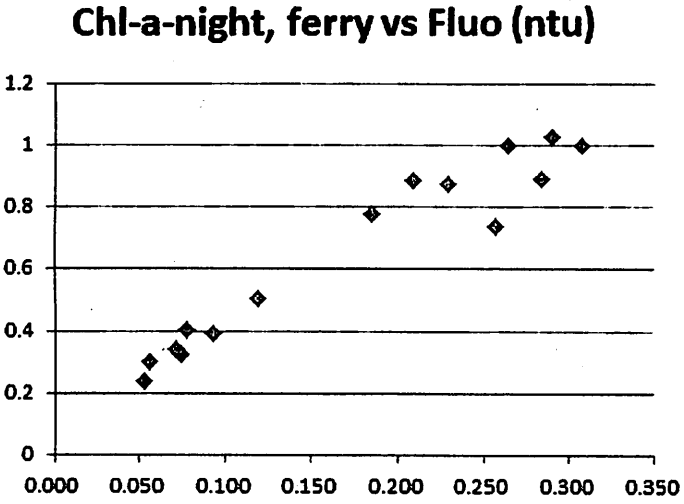

Fig 6: Nighttime Chl-a data from ferry and from NTU's bottled water.

The Chl-a from sensor on the ferry gave much higher values than those from the bottled data. The source of difference may be (1) sensor drift, (2) different units. Verification will be made after filling in the Chl-a data from Nagoya University.

It is clear that most of the data has a nearly linear relationship, but the daytime pair of data and nighttime pair of data shows slightly different regression relation.

For the daytime data of May 13, the ferry Chl-a*0.225+0.07 and sea surface temperature (SST) were plotted against time in Figure 7.

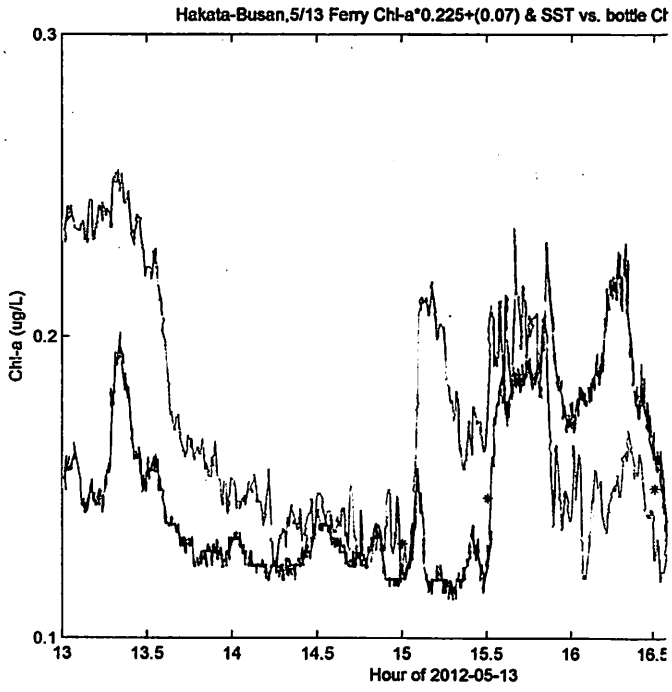

Fig 7: Time series plot of the day time Chl-a*0.225+0.07 (blue curve) and the sea surface temperature (SST, green curve), and the Chl-a (red *) from NTU's bottled water.

The continuous ferry Chl-a data correlates well with NTU's Chl-a, except at 17:00 of May 13.

The latitudinal variation of modified ferry Chl-a (blue), the SST (green), and NTU's Chl-a from bottled water are shown in Figure 8, for the survey on May 13, from Hakata to Busan.

In general, the Chl-a is high in coastal water of Japan and Korea, and near Tsushima Island, and Chl-a is low in deep channels on both sides of Tsushima Island.

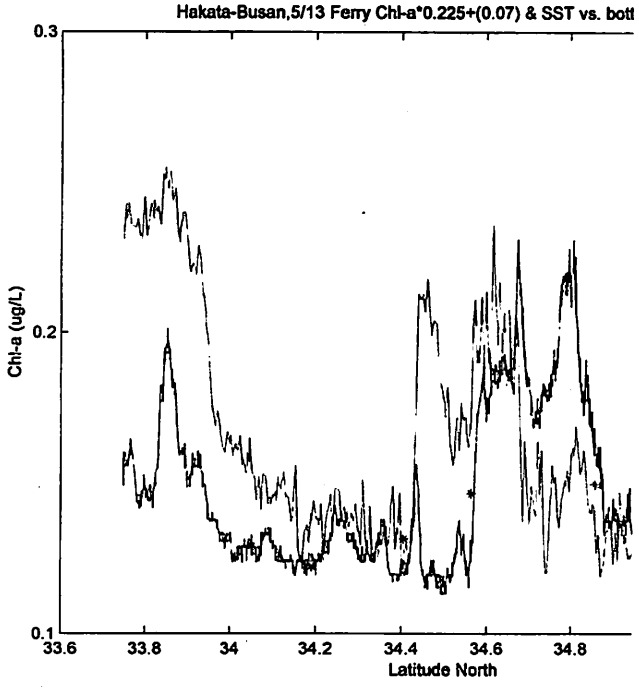

Fig. 8: Latitudinal change of Chl-a (blue for ferry data, and * for NTU data) and SST (green curve) from Hakata to Busan on May 13 of 2012.

Away from the coast, there is no sign of correlation between the salinity of surface water and the Chl-a centration. But, near the coast of Japan and of Korea, the water is less saline due to river run-off, and the Chl-a increases as one gets closer to the coast (Figure 9) because the river water has much higher Chl-a concentration.

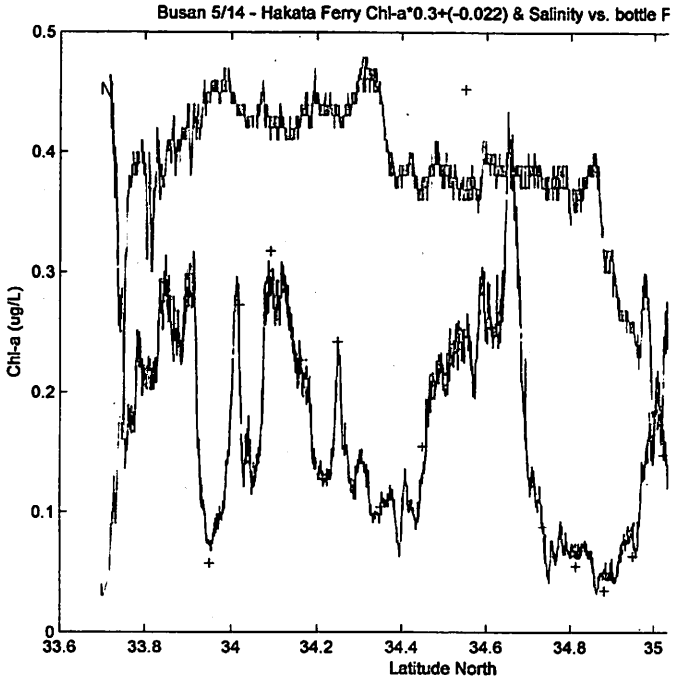

Fig. 9: Plot of Chl-a (blue curve for sensor data, + for bottled data), and salinity (green curve) as a function of latitude.

The spatial variation of Chl-a may be seen by overlaying the sensor data of Chl-a on the satellite-derived Chl-a concentration (all satellite images are provided by Prof. Joji Ishizaka), as seen in Figure 10. Sensor data were taken in the afternoon of May 13, while the satellite image was at 2pm of May 15.

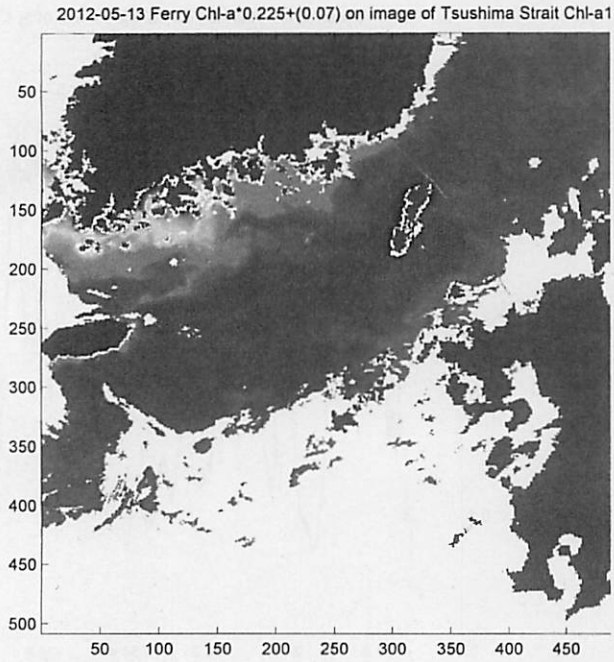

Fig. 10: Chl-a data from sensor on New Camellia of May 13 is overlaid on satellite-derived Chl-a distribution over Tsushima Strait on May 15.

A better comparison is using sensor data at pre-dawn of May 15 overlaid on satellite image at 2pm of May 15, as in Figure 11a. Over the west channel, the cruise track is nearly invincible, which means that the sensor data agrees well with satellite data of Chl-a.

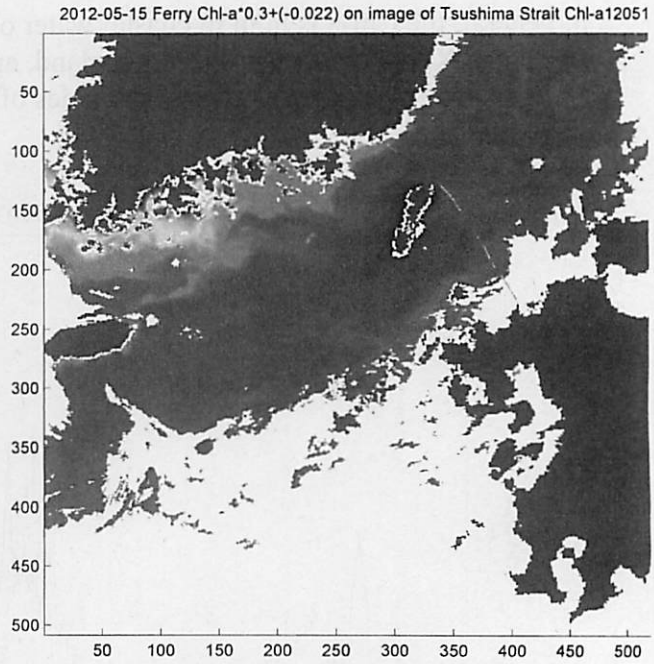

Fig 11a: Same as Fig 10, except Chl-a sensor data at 2pm of May 15.

Figure 11b uses satellite image at 2pm of May 17. In Figure 10-11, the Chl-a from sensor data seems to be equal or larger than satellite Chl-a data.

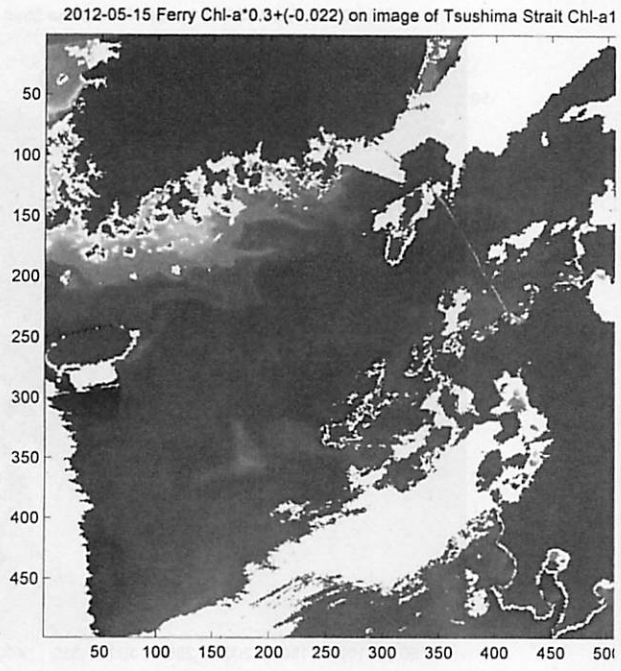

Fig 11b: Same as Fig. 11, except satellite Chl-a data at 2pm of May 17.

An easier comparison is the sensor SST and satellite-derived SST. It is easy because both ferry SST and satellite SST have smaller uncertainty than Chl-a data. The ship track can hardly be seen in Figure 12. It means that the ferry SST of May 13 afternoon is nearly the same as satellite SST of May 15 afternoon.

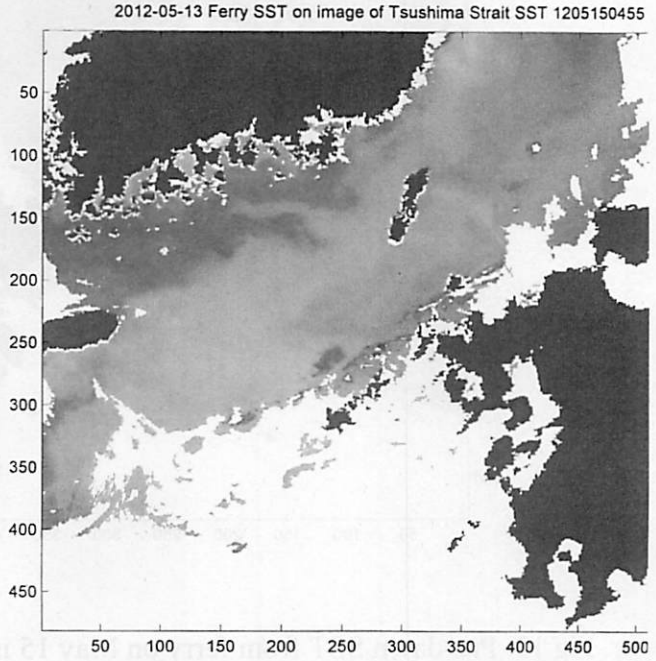

Fig 12: Afternoon SST from ferry on May 13 is plotted against satellite-derived SST at 2pm of May 15.

The ferry SST at pre-dawn of May 15 seems to be lower (SST along ship track seems darker than the background, or the satellite SST) than satellite SST of May 15 2pm.

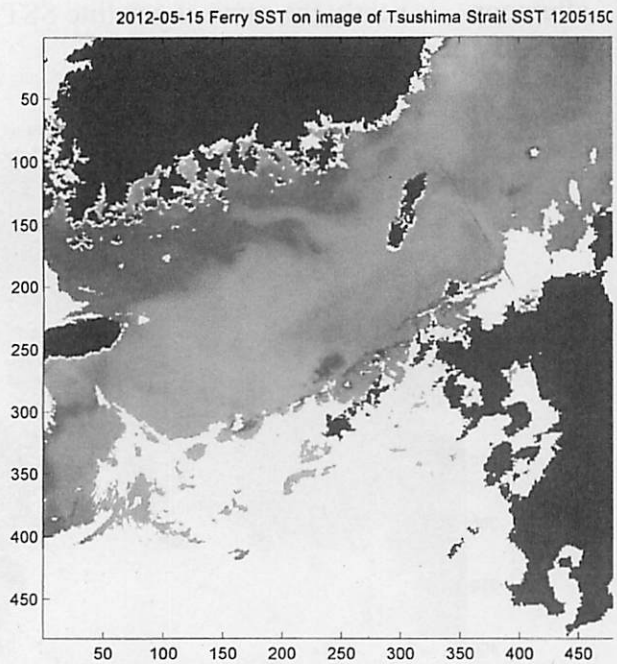

Fig 13: Pre-dawn SST from ferry on May 15 is plotted against satellite-derived SST at 2pm of May 15.

The satellite SST of May 17 (Figure 14) is greenish that Figure 13. This may be the reason that the ship track can hardly be seen in Figure 14.

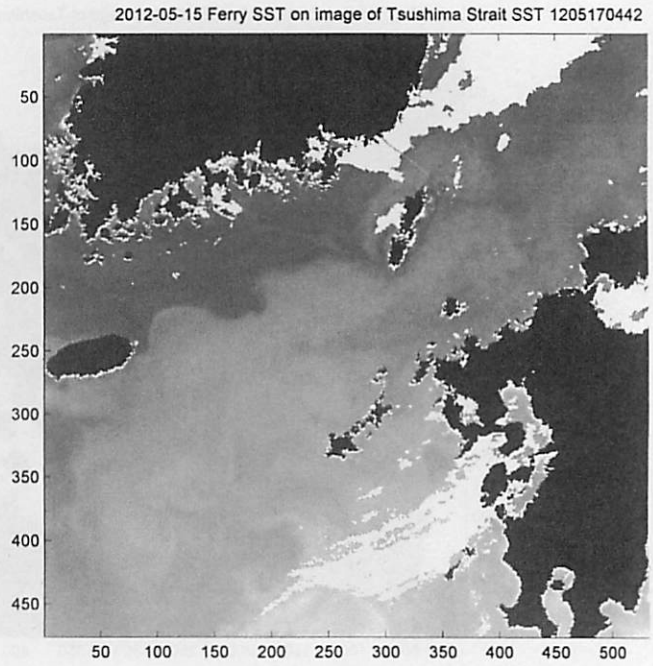

Fig 14: Pre-dawn SST from ferry on May 15 is plotted against satellite-derived SST at 2pm of May 17.

Conclusion

1. The Chl-a sensor on New Camellia is healthy, because its data varies linearly with the Chl-a from bottled data.

2. Sensor-drift happens to the Chl-a sensor on New Camellia. Regular calibration seems necessary for accurate data.

3. The Chl-a concentration correlates well with sea surface temperature (SST), Chl-a is higher in regions with lower SST. This phenomenon was also observed in earlier studies.

Suggestions:

1 Calibration of Chl-a sensor may be partially replaced by comparing sensor data with that of satellite ocean color images that has accuracy of 30%.

2 In taking water samples, a clear bottle may be better than both big cup and brown bottles;
a clear bottle permit filling the bottle faster, and shaking before filtering;
(this will prevent phytoplankton from floating on water surface, or adhering to the bottle)

国際化推進共同研究概要

No. 3

タイトル： Effects of tansmutant helium on the microstructure of fusion reactor structural materials.

研究代表者：ODETTE, George, Robert

所内世話人：渡辺　英雄

実 施 期 間：2012年9月21日 ～ 9月28日

研 究 概 要：核融合炉低放射性構造材料の損傷評価には核変換により形成されるヘリウムとははじきだし量(dpa)との関連が重要である。本研究は、ＵＣＳＢが保有する各種の材料にたいして、九州大学・応用力学研究所が所有するタンデム照射を始めとする各種照射実験を通して、重畳効果を明らかにする事を目的としている。今年度は、スウェリング機構の中核をなすヘリウムバブルからのボイド発生の過程の詳細を明らかにするために 、ヘリウム注入後の試料の高圧電子線照射及び顕微鏡観察を行った。

Effects of tansmutant helium on the microstructure of fusion reactor structural materials

T. Yamamoto, Y. Wu, G. R. Odette (University of California Santa Barbara), H. Watanabe (Kyushu University)

Introduction

One of the challenges that fusion reactor materials development faces is to manage and mitigate the possible effects of transmutation He on the mechanical properties of first wall structural materials. In a typical DEMO fusion reactor design, after a year of operation at a neutron wall load of 5 MW/m^2, ≈ 500 appm He will be generated in Fe-based materials as well as displacement damage of ≈ 50 dpa. Helium bubbles form in the matrix as well as on dislocations, precipitate interfaces and grain boundaries (GB) [1]. A physically motivated analysis of limited data in the literature for fracture toughness transition temperature shifts (ΔT), led to our proposed model predicting very large ΔT at low irradiation temperatures in tempered martensitic steels (TMS), due to irradiation hardening ($\Delta\sigma_y$) coupled with GB He embrittlement [2-3], that has been confirmed in the later experiments [4]. More recent experiments in HFIR reactor using in situ He implanter (ISHI) technique have shown that in TMS F82H and Eurofer 97 relatively large He bubbles form at mainly dislocations and lath boundaries leading to void nucleation even before ≈ 10 dpa at the He/dpa ratio of 40 appm. Figure 1 shows cavity microstructure in F82H after irradiation to 9 dpa as well as He implantation to 380 appm at 500 °C. There is a distinct bi-modal cavity size distribution that consists of numerous small bubbles with average diameter of ≈ 2 nm in the form of string-of-peals like chains and fewer large faceted cavities, which are likely voids [5]. The voids can nucleate at bubbles that has reached a critical size, then continuously grow increasing the volume fraction of cavities, corresponding to void-swelling, to ≈ 0.5% at 21 dpa [6]. Such He-dpa synergistic effects on the swelling that is life-limiting factor in the intermediate temperature range has to be understood and modeled accurately to predict the structural performance during the fusion reactor operation, along with the low temperature embrittlement and high temperature creep behavior.

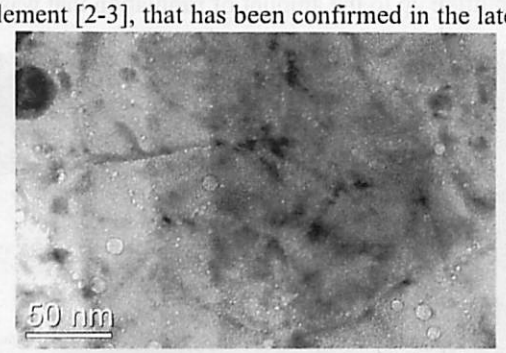

Figure 1 Cavity microstructure in F82H after in situ He implantation to 9 dpa and 380 appm He at 500 °C in HFIR, showing numerous small bubbles mostly formed on dislocations as string-of-pearls like chains with fewer large faceted cavities which are likely voids [5].

The fundamental overriding questions about He-dpa synergisms include: a) What are the basic interacting mechanisms controlling He and defect transport, fate and consequences, and how are they influenced by the starting microstructure and irradiation variables (dpa rate, He/dpa ratio, temperature and applied stress); and, b) how can the detrimental effects of He-dpa synergisms be mitigated and managed by proper microstructural design? Our approach to answering these questions is to build experimental knowledge base through the experiments in wide ranges of material and environmental variables, that is coordinated with development of physically based models of the microstructural evolution. The objective of this research is to examine He behavior in the materials during various charged particle irradiations, that provide experimental data for very wide ranges of damage level (dpa) and He-to-dpa ratio as well as the mechanistic insights.

Experimental techniques

As mentioned above we have demonstrated that ISHI method in mixed spectrum fission reactor irradiations provides a very attractive approach to assessing the effects of He-dpa synergisms, while avoiding most of the confounding effects associated with Ni- or B-doping type experiments [1,5-9]. The technique can generally probe the He/dpa range of 10 to 60 appm at a damage level higher than 5 dpa at damage rate of ≈ 10^{-6} dpa/s. Another approach is to use spallation proton irradiation such as STIP, spallation target irradiation program. A high energy (≈ 600MeV) proton beam produces significant amount of He as well as displacement damage in target materials generally at a rate from 50 to 100 appm He/dpa for damage levels > 5 dpa. Heavy ion (such as Fe^{3+}) beam irradiation is also widely used to produce displacement damages in materials. In dual or triple ion (DI, TI) beam facilities, an additional use of a He ion beam can produce He/dpa up to ≈ 100 appm/dpa. Single ion irradiation of He can implant a large amount of He while introducing relatively small amount of displacement damages, which results in very high He/dpa ratio up to ≈ 10^4 appm. Further, high voltage electron microscopy (HVEM) can introduce additional displacement damages to the specimen while observing the microstructure evolution. Combinations of these various techniques allow us to probe the effects of wide ranges of irradiation variables on microstructure evolution in the target materials. This year we have focused on the mechanisms of void nucleation and growth from the population of He bubbles. F82H specimen previously

irradiated to 10 dpa and 400 appm He at 500 °C in dual ion beams of He^{+} and Fe^{3+} in the DuET facility at Kyoto University [10] was observed in HVEM while further displacement damage being introduced by 1000 kV electron beam irradiation.

Results

Figure 2a shows cavity microstructure of the F82H specimens after DuET irradiation to 10 dpa and 400 appm He at 500 °C. Bubbles with average diameter of ≈ 3 nm to ≈ 5 nm, depending on the depth from the surface, were observed at the number density of ≈ 5 x 10^{22} m^{-3} over the depth range from 500 to 1500 nm. Electron beam irradiation along with observation was performed to cover the depth range. Figures 2b and 2c show snap shots of the microstructure evolution during the electron beam irradiation after b) 2 min (0.04 dpa) and c) 3 hours (3 dpa). The pictures cover the depth range from near surface to ≈ 1500 nm. While the images were taken at slightly under focus condition, no void formation or growth was observed under the imaging condition up to the amount of irradiation that was achieved within our allocated machine time.

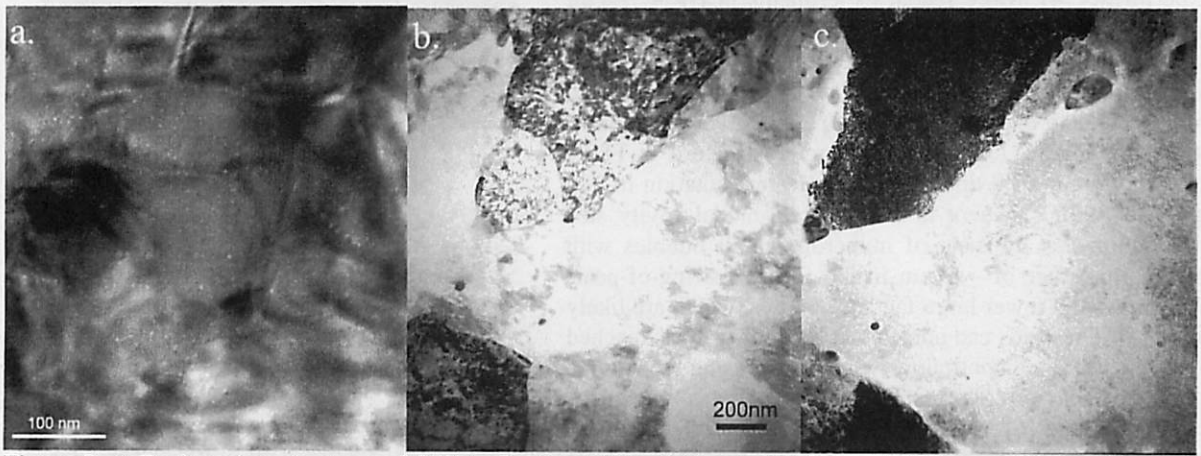

Figure 2 a) Cavity microstructure of F82H after DuET irradiation to 10 dpa and 400 appm He at 500 °C, b) Cavity microstructure during 1000kV electron beam irradiation at damage rate of 3 x 10^{-4} dpa/s at 500 °C to ≈ 0.04 dpa and c) to ≈ 3 dpa.

Summary and future plan

We have performed 1000 kV electron beam irradiation for tempered martensitic steel F82H, previously irradiated to 10 dpa with 400 appm He at 500 °C in a dual ion beam facility DuET, Kyoto University. We will analyze the post-irradiation cavity structure using high resolution TEM as well as to perform further HVEM irradiation to obtain information on void nucleation and growth from the He saturated bubbles.

Acknowledgements

Authors are grateful to Professor Kimura and Dr. Kondo at Kyoto University for DuET irradiation. Part of the research performed by UC Santa Barbara participants is supported by US DOE.

References:

1. Y. Dai, G. R. Odettte, T. Yamamoto, *The Effects of helium on irradiated structural alloys* in: R.J.M. Konings(ed.) Comprehensive Nuclear Materials, volume 1, pp. 141-193 Amsterdam: Elsevier (2012)
2. T. Yamamoto, G.R. Odette, H. Kishimoto, J-W. Rensman, P. Miao, J. Nucl. Mater. **356** (2006) 27.
3. G.R. Odette, T. Yamamoto, H.J. Rathbun, M.Y. He, M.L. Hribernik, J.W. Rensman. J. Nucl. Mater. **323** (2003) 313.
4. T. Yamamoto, Y.Dai, G. R. Odette, M. Salston, P. Miao, Trans. American Nuclear Society, 98 (2008) 1111.
5. T. Yamamoto, G.R. Odette, P. Miao, D. J. Edwards, R. J. Kurtz, J. Nucl. Mater., 386-388 (2009) 338.
6. G.R. Odette, P. Miao, D.J. Edwards, T. Yamamoto, R.J. Kurtz, H. Tanigawa, J. Nucl. Mat. 417 (2011) 1001.
7. T. Yamamoto, G.R. Odette, L.R. Greenwood, DOE/ER-313/38(2005) 95.
8. T. Yamamoto, G.R. Odette, P. Miao, D. T. Hoelzer, J. Bentley, N. Hashimoto, H. Tanigawa, R. J. Kurtz, J. Nucl. Mater., 367 (2007) 399.
9. G.R. Odette, M.J. Alinger, and B.D.Wirth, Annu. Rev. Mater. Res. 38 (2008)471.
10. T. Yamamoto, Y. Wu, G.R. Odette, K. Yabuuchi, S. Kondo, A. Kimura, Fusion Materials Semiannual Report 6/30/2012 DOE/ER-313/52 (2012) 8.

国際化推進共同研究概要

No. 4

タイトル： Development of high-power ECRH transmission and launcher for ITER

研究代表者：KASPAREK, Walter, Hermann

所内世話人：図子　秀樹

実 施 期 間：2013年3月10日 ～ 3 月12日

研究概要：　国際熱核融合実験炉(ITER)では、電子サイクロトロン加熱(ECH)によるプラズマ生成・加熱、電流駆動が計画されている。ITER　におけるECH システムでは、170GHz CW ジャイロトロン管で発振される1MW の大電力高周波が用いられる。ITER ECH システムでは、ジャイロトロン管で発振した大電力高周波は、伝送路でアンテナへと送られ、プラズマに放射される。伝送路は、オーバーサイズ導波管による要素部品で構成されており、伝送路のミスアライメント等で、主伝送モード以外の不要高次モードも励起される。励起されたモード間干渉により、伝送路でのアーキング、過熱が発生する。本研究では、伝送路のモードを測定できるモード分析器を試験・開発することを目的とする。　不要な高次モードは大別すると、主要伝送モードと異なって非軸対称な電界分布を持つモード、軸対称な電界分布を持つものの導波管径方向に異なる電界広がり持つモードがある。前者は、主にジャイロトロン管から導波管伝送路への結合軸ミスアライメントで、後者は結合ビーム径、位相分布のミスマッチングで生ずる。昨年度、提案されたモード分析器の熱応力解析を行った。導波管伝送路に設置される９０° ベントの反射板に結合孔列をもつ副導波管回路を反射板中心位置、中心から外れた同心円位置に置く構造であるが、反射板中心位置で熱応力集中がおき、結合孔部が損傷すると解析された。軸対称な電界分布を持つ不要モードの同定には、反射板中心位置の副導波管回路が必要なため、新たな概念に基づく分析器の開発が必要となった。モードの位相が反転する位置に副導波管回路をおくことを着想し、高周波動作評価、熱応力解析を進め、ITER での 2MW 伝送で２電界方向４モード（計８成分）計測を行える分析器設計を終えた。モード分析器の設計をモード分析器の評価には、基準となるモード発生器の開発が不可欠であるが、ドイツで共振器原理を用いたモード発生器、九大では２ガウスモード整合

に基づくモード発生器の開発を進め、いずれも 96 % 以上のモード純度が達成されることを実験的に検証した。

Report on High-power ECRH Transmission and Launcher

Applicant: Walter Kasparek

Institute of Interfacial Process Engineering and Plasma Technology (IGVP)

The work performed under support of the Collaborative Research Program of the Research Institute for Applied Mechanics, Kyushu University, dealt with methods to characterize oversized corrugated transmission lines and launchers in high-power ECRH systems. Especially, the work performed under the collaboration aimed at the development of a high-purity HE11 mode generator and a coupler for alignment control and wrong mode detection in corrugated HE11 lines.

The International Joint Research team consisted (besides the applicant) of Hiroshi Idei (RIAM, Kyushu), Keishi Sakamoto (JAEA Naka), Takashi Shimozuma (NIFS, Toki), Richard Temkin (MIT PSFC Cambridge), Michael Shapiro (MIT PSFC Cambridge), Carsten Lechte (IGVP Stuttgart), and Burkhard Plaum (IGVP Stuttgart).

A first task in this collaboration aimed at transmission-mode monitoring, alignment control and wrong mode detection in corrugated HE11 lines. In close cooperation, 5-port coupler systems, which are integrated into a miter bend of the corrugated HE11 transmission line, where developed. Design optimizations have been performed, showing that by choosing proper positions for the coupling holes and with an appropriate signal processing, it is possible to obtain the amplitudes of 5 modes with a 5-port coupler. Especially, if the coupler structures are optimized to detect - besides the fundamental HE11 (LP01) mode - the first higher-order symmetric LP02 mode and the first asymmetric modes LP11 (odd) and LP11 (even), then the essential basic information needed for operation of the line, namely power (from the HE11 signal), diameter matching of the gyrotron beam (from the LP02 signal), and possible misalignments (from the LP11 signals) can be obtained.

In last year, two prototype mitre bend mirrors with integrated couplers have been built. The first is adapted to the parameters of the ASDEX Upgrade ECRH system (140 GHz, waveguide diameter 87 mm), and is not cooled, which eases design and fabrication. This coupler has been investigated in detail during the time of the collaboration. In this year, the thermal stress due to the temperature increment has been analysed with a finite element code. 2MW H-plane transmission was considered for an application to the ITER ECRH system. It has been found that the couplers which are centrally located at the mitre bend mirror might be damaged by the stress. A new coupler system has been designed in this year. 8-port couplers have been considered to detect the 3 spurious modes as well as the dominant LP01 mode in two orthogonal electric field components. The new couplers are located at π phase-jumping positions and are not centrally located at the mitre bend mirror; they can detect each specific mode by one coupler without signal processing. The RF performance and thermal stress were evaluated. This mirror is going to be ready soon, and is waiting for low-power tests at RIAM, and a possibility for high-power testing at the 170 GHz ITER test stand at JAEA in Naka.

For the test of advanced HE11 transmission lines, mode generators with very high mode purity were developed which are compatible with the present ITER ECRH system (170 GHz, waveguide diameter 63.5 mm). Two approaches were pursued.
A resonator, which uses the HE11 field as an eigenmode, was designed and built. It consists of two mirrors, a phase-reversing mirror designed for the HE11 mode field, which is defined according to the waveguide parameters on the interface plane between resonator and waveguide, and a semi-transparent plane mirror as output coupler. The excitation of the resonator was performed via a shallow phase grating and a Gaussian feed horn. Detailed measurements of amplitude and phase of the output fields, and evaluation of the efficiency and mode purity have been performed, showing that a good HE11 beam was generated. However, interference occurred with the excitation beam via the semi-transparent mirror, and thus reduced the final mode purity of 96 %. As countermeasure, the feed structure is changed to a classical beam splitter, where the interference between output beam and exciting beam is avoided. This modification is underway.
The second approach was based on a synthesis of the HE11 pattern starting from the (very similar) Gaussian beam. The horn to produce this beam was calculated, and a phase-matching system based on the Kirchhoff integral on the HE11 high mode-purity generator was designed. 2 Gaussian beams expanding and focusing are merged to generate the high purity HE11 mode. The mirror performance has been explained well by the moment-method simulator. A very high performance with a mode purity of better than 99.8% is calculated. This generator was designed, fabricated and was tested in Kyushu University. A mode purity of 97 % has been achieved in this generator. The discrepancy with the calculations is due to the wire-grid polarizer, which was used to merge the 2 Gaussian beams. The diameter of the wire-grid polarizer is about 170 mm, and the uniformity of the wire-grid spacing degrades at the centre due to low tension to put the wire-grid to the polarizer frame. A support wire structure has been designed and a new polarizer was fabricated, and is waiting to be tested.

The results on the work on 5-port couplers were published in a refereed journal as follows: J. Ruiz, W. Kasparek, C. Lechte, B. Plaum, and H. Idei, "Numerical and experimental investigation of a 5-port mitre-bend directional coupler for mode analysis in corrugated waveguides". Journal of Infrared, Millimeter, and Terahertz waves 33: 491–504 (2012). Also, the results on the HE11 mode generator based on 2 Gaussian beams were published in a refereed journal as follows: "M. Sakaguchi, H. Idei, *et al.*, "Quasi-Optical High Purity HE11-Mode Exciter for Oversized Corrugated Waveguide Transmission", Plasma and Fusion Research Volume 7, 2405037 (2012).

To summarize, the collaborative work resulted in appreciable success in the design of components for high-power ECRH transmission lines. The 2MW transmission capability was taken as basis for the design of the transmission-mode monitoring system in the ITER ECRH system. For the reliable operation of ITER, alignment control and wrong mode detection in corrugated HE11 lines is so important in "High-power ECRH Transmission and Launcher". This collaboration has been concluded, taking a new progress of high power transmission-mode monitoring.

国際化推進共同研究概要

No. 5

タイトル：Turblence and zonal flow data analysis and experimental plan of HL-2A tokamak

研究代表者：DONG, Jiaqi

所内世話人：藤澤　彰英

実 施 期 間：

研 究 概 要：中国の西南物理研究所の HL-2A トカマクの周辺の乱流データの解析を共同で行った。今回は磁気島の乱流に及ぼす影響について特に研究を進め初期的な解析と今後の方針が固まった。

共同研究課題名　**「HL-2A トカマクにおける乱流と帯状流に関するデータ解析と実験計画」に関する報告**

（英文課題名　Turbulence and zonal flow data analysis and experimental plan of HL-2A tokamak）

世話人　藤澤彰英

1. 共同研究の目的

プラズマ乱流は磁場閉じこめプラズマの閉じこめ性能を決める重要な因子であり、長年にわたり国際的に研究されてきた。近年の研究で、乱流が帯状流（メソスケール）や更にマクロな揺らぎ構造を生成することが明らかになり、この新しい概念に基づいた乱流研究が世界各国で行われている。中国の西南物理研究所にある HL-2A トカマクで多チャンネルプローブによりプラズマ周辺の乱流と帯状流（GAM を含む）を精力的に行い貴重なデータを得ている。これまで応力研プラズマ乱流研究グループで開発してきたプラズマ乱流や帯状流の先進的な解析法を、HL-2A のデータに適用し、プラズマ乱流の研究を推進するために西南物理研究所の共同研究の代表者 Dong Jiaqi 教授たちと平成２３年度以降、国際ワークショップを開催している。今回、応用力学研究所の援助を得てこの共同研究を推進した。

2. 共同研究の成果

今回は、中国からは来日のビザが発行されない等のトラブルがあり、当初予定の Dong 教授の来日がかなわなかったが、韓国在住の Zhao 博士が応力研を訪問した。その際、HL-2A の最新のデータを用いて共同研究を行った。

今回の共同研究では、プラズマの周辺領域にある磁気島の周りに、いくつかのモード(5.5kHz, 10.5kHz, 12kHz)が相互作用し共存している複雑な状態が見つかり、これらのモードと乱流との相互作用、磁気島がこれらのモードに及ぼしている影響、あるいは磁気島まわりの乱流特性などについて調べることを行った。

まず、第一に、これらのモードの時空間構造（径方向およびトロイダル方向）について調べ（図１参照）、①10.5 kHz のモードは空間構造の異なる２つのモードから構成されていること、②GAM(m=0)と 5.5kHz２倍高調波(m/n=6/2)とから

なること、③5.5kHz の揺動はティアリング・モードであること、が示唆された。

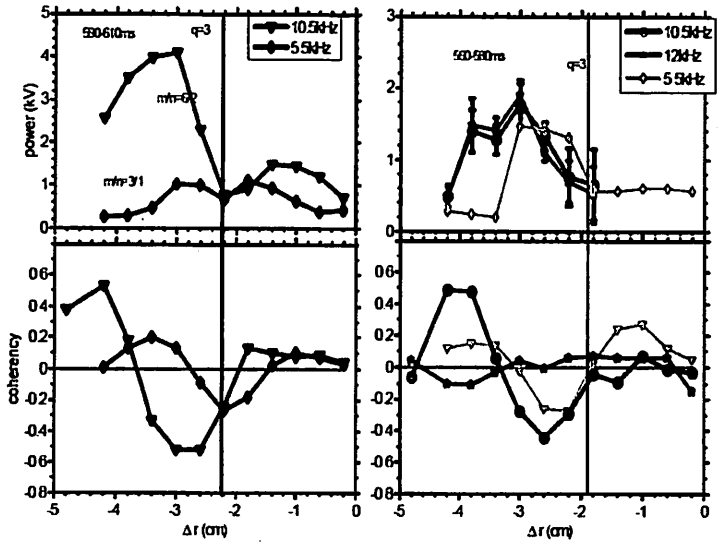

図.1　複数のモードが競合する HL2A の放電。それらのモードの空間分布

特に、２つの異なるモードが競合していると思われる 10.5kHz 領域については、磁気プローブとの相関を取ることで、モードを分離することができると考えられることまた、磁気島の乱流への効果として乱流強度のモジュレーションが期待されるが、磁場揺動（ティアリング・モード）や電位揺動とのエンベロープの時間変化の比較を行うことで、磁気島の磁場トポロジーと乱流の関係が調べられること、が議論された。また、これらのモードは時間的には定常ではなく間欠的な性質を持っているので、その出現している時刻に関して解析を行うことでより精度の高いデータとなるだろう、との議論がなされた。

3. 今後の課題と計画

これまで西南物理研究所のメンバーとの共同研究は古く数編の共著論文(K. J. Zhao et al., Phys. Rev. Lett 96 255004 (2006), K. J. Zhao et al, PPCF 52 124008 (2010)ほか)が出版されている他、2012 年に IAEA 主催で開催された Fusion Energy Conference などに共著論文が受理されている。今後も本課題の下、共同研究を続けてゆく。実際には e-mail などにより、コミュニケーションを行い、効率化を図る。

国際化推進共同研究概要

No. 6

タイトル：Comparative and joint study of steady state operation(SSO) of high temperature plasmas and related plasma wall interaction(PWI) on QUEST and EAST.

研究代表者： GAO, Xiang

所内世話人：花田　和明

来訪期間 ： 2013 年 3 月 13 日 ～ 3 月 20 日

概要： 昨年度実施した実験結果を Journal Nuclear Material 誌に投稿し、掲載が確定した。更なる論文投稿を行うためのデータの解析についての議論のために3月に来訪予定である。来訪後に改訂した報告書を再度提出の予定である。

RESEARCH REPORT

Date Mar. 24, 2013

Visiting scientists: (name) Xiang Gao

(position) Professor

(university / institute) Institute of Plasma Physics,
Chinese Academy of Sciences

(name) Yinxian Jie

(position) Professor

(university / institute) Institute of Plasma Physics,
Chinese Academy of Sciences

(name) Haiqing Liu

(position) Associate Professor

(university / institute) Institute of Plasma Physics,
Chinese Academy of Sciences

Host scientist: (name) Kazuaki Hanada

(position) Professor

(university / institute) Kyushu University

Research period: (from) Mar. 13, 2013 (to) Mar.20, 2013

Research subject: **Comparative and joint study of steady state operation (SSO) of high temperature plasmas and related plasma wall interaction (PWI) on QUEST and EAST**

Introduction

Steady state operation (SSO) of tokamak plasma is one of the basic requirements for future fusion reactors. The mission of QUEST is to develop the scientific basis for achieving a steady state condition at sufficiently high beta (~20%), with high confinement and low collisionality. The mission of the EAST project is to study the physical issues involved in steady state advanced tokamak devices. QUEST is a Sperical tokamaks(ST) which has the possibility to realize cost-effective fusion power plants because of High β is the indispensable target ; the use of full superconducting poloidal field coils on EAST is the first trial test in the world for the sake of international thermonuclear experimental reactor (ITER). Comparative and joint study on QUEST and EAST is most important thing because the special feature of these two devices (QUEST, SSO with High beta; EAST, SSO with full superconducting coils). All sub-issue studies aim to achieve SSO plasma in QUEST and EAST, and contribute to ITER. Exploitation and integration of diagnostic system resources in these two devices and compare the two-side result would have give many fruitful results. Recently, in particular for fusion, is further amplified by similarities between blobs and ELM filaments, which suggest that the same mechanism is governing their dynamics. To do the comparison studies of blobs in QUEST, HT-7,EAST and ELMy filaments in EAST is approachable way to find their mechanism in near future. This comparative and joint research would have provided many fruitful results in these research fields.

Recently experimental results in QUEST and EAST

Towards SSO of a ST on QUEST, Zero-dimensional calculations of particle balance for QUEST experiment was done, refresh wall, and hot wall were performed showing that a SSO time of more than 1000s is required to obtain reliable results in regard to particle balance, as shown in Fig.1 (*Hanada et al., IEEEJ, 2012*). The number of stored particles depends on the targeted wall temperature. The hot wall around 673K could not have the property of pumping.

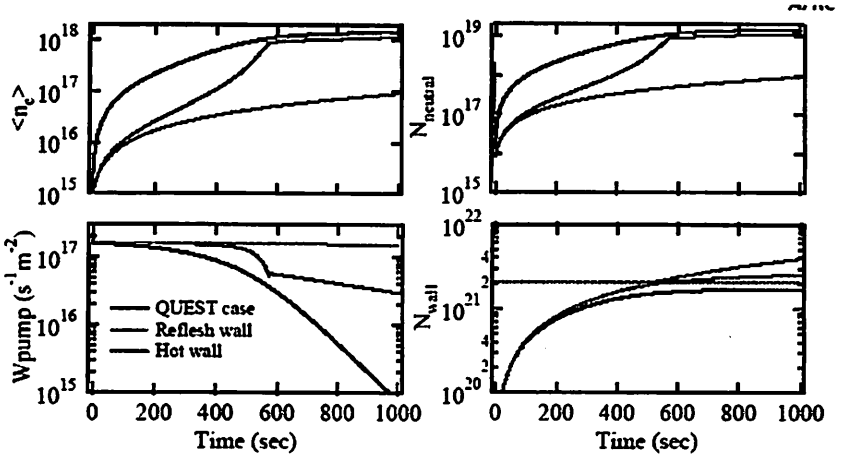

Figure 1 Steady state will be realized more than 1000s. (Hanada et al., IEEJ Transactions on Fundamentals and Materials; ISSN:0385-4205; VOL.132; NO.7; PAGE.490-498; 2012).

On QUEST, a spherical tokamak configuration with the aspect ratio of less than 1.5, the plasma current up to 25kA could be obtained for 1s by fully non-inductive current drive using the well-controlled microwave of 8.2GHz, 120kW. The plasma of more than 10kA, A~1.5 could be obtained by only 8.2GHz microwave on a limiter configuration, as shown in Fig.2. The non-inductive current is driven by toroidally asymmetric orbit of energetic electrons accelerated by the microwave. The plasma current was reduced by the increment of out-gassing caused by the presence of the hot spots made by direct attack the energetic electrons on the wall. The single-null divertor configuration was formed and could be maintained for 20 sec. Ion saturation current measured on the divertor plate surface was increasing around the divertor leg. QUEST experiments have opportunity to challenge for SSO of ST, as shown in Fig.3.

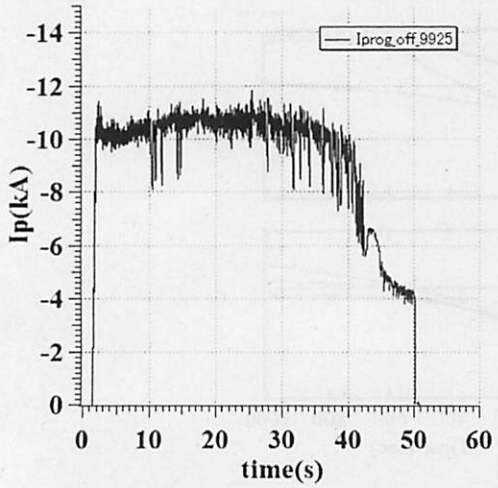

Figure 2 37s steady state operation on QUEST. (Hanada et al., presentation in discussions)

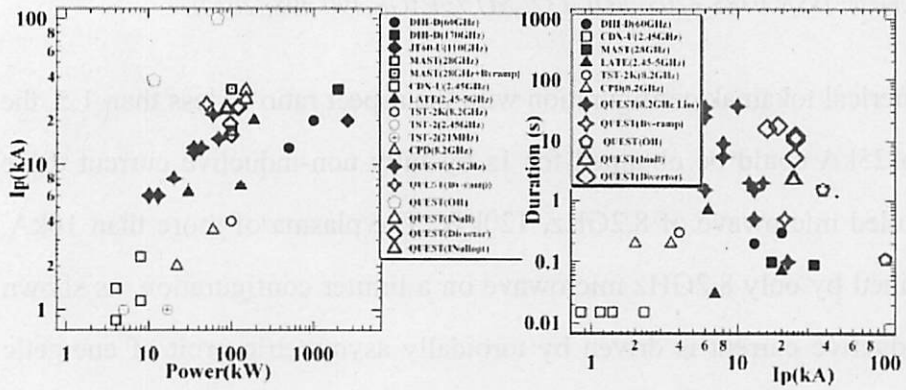

Figure 3 Development of QUEST status (Hanada et al., presentation in discussions).

EAST is a non-circular full superconducting tokamak device. The missions of EAST are to play the key role for understanding advanced SSo plasma physics and to provide valuable data bases for ITER under ATSSO condition. The target of EAST are 1MA SSO with 20-30MW CW Heating & CD power and more than 50 diagnostics . In 2012, the water-cooling Mo wall was installed in EAST as shown in Fig.4.

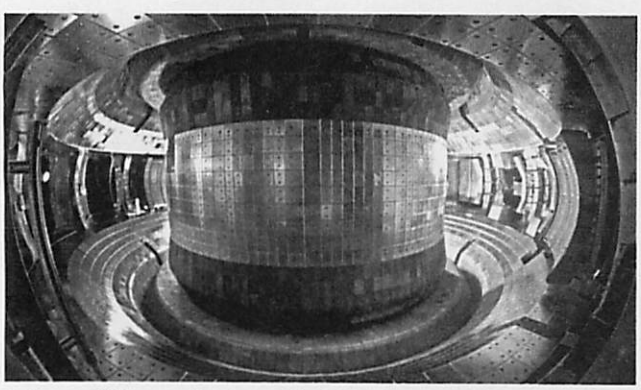

Figure 4 The actively cooled Mo first wall in 2012 on EAST.

During the experimental campaign in 2012, with actively realtime Lithium wall coating and RTEFIT/Isoflux control, 411s long pulse high temperature divertor plasma discharge was achieved on EAST. Along accumulation of Lithium in vessel, stationary ELMy H-mode plasmas (up to 32 s) have been achieved on EAST by the combination of ICRF heating and LHCD with Ip = 280 kA, a toroidal field of 1.85 T at R = 1.75 m, a line averaged density of 2×10^{19} m^{-3}, P_{LH} ~ 2.0 MW, P_{ICRF}~0.75MW, Beta_P ~ 1.0, H_{98} ~ 0.8, as shown in Fig.5. Discharge with a plasma current of 1 MA was realized on EAST. It established a good base for further high-performance plasma study in the near future.

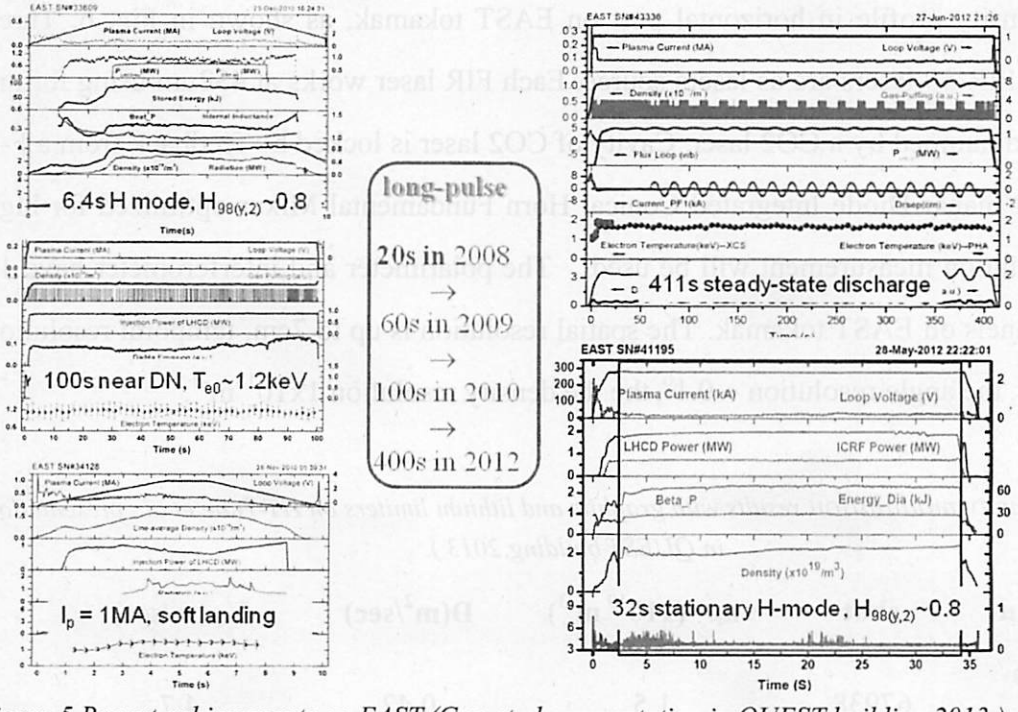

Figure 5 Recent achievements on EAST (Gao et al., presentation in QUEST building,2013).

Particle confinement study is a very important issue for magnetically confined plasmas. Density modulation is a powerful approach to solve the experimental difficulties in particle confinement experimental studies. In 2011, the density modulation experiment with the lithium limiter was performed and compared with the results of graphite limiters on HT-7. The major difference is in convection velocity, V, measurement. And a stronger pinch effect has been observed in 2011. The V measurements on two density platform values both suggest that the lithium limiter could improve the particle confinement, as shown in Table 1.

The further density modulation experiment was done on EAST and in analyzing, would contribute to the SSO on EAST.

Plasma activities associated with current density profile and electron density profile, the current density profile is key parameter for real-time plasma control (q profile and current density relaxation) for long-pulse discharges: connect plasma (diagnostics) – PCS - actuators (ICRH,LHCD) - plasma response and extend high-performance plasma regimes to long-pulse in preparation for ITER. The polarimetric and interferometric measurement with high temporal, spatial and angle resolution are required on EAST. A new three-wave polarimeter and interferometer will be setup to measure plasma current density profile and electron density profile in horizontal port on EAST tokamak, as shown in Fig. 6. Three coherent SIFIR-50 lasers are as lasers source. Each FIR laser works at 432um using formic acid gas and pumped by a CO2 laser. Cavity of CO2 laser is locked by feedback from a F-P cavity. VDI planar-Diode Integrated Conical Horn Fundamental Mixer optimized for high spatial resolution measurement will be used. The polarimeter and interferometer have 11 lateral channels on EAST tokamak. The spatial resolution is up to 7cm, temporal resolution is up to 1us, the angle resolution ~ 0.1°, the the density resolution $1x10^{18}m^{-3}$.

Table 1 Density modulation results with graphite and lithium limiters on HT-7(Jie et al., presentation in QUEST building,2013).

Without lithium limiter	**shot**	**$<n_e>$ ($x10^{19}$ m^{-3})**	**$D(m^2/sec)$**	**V_0 (m/sec)**
	67938	1.5	0.42	4.7
	67941	2.2	0.28	-0.4
With lithium limiter	**shot**	**$<n_e>$ ($x10^{19}$ m-3)**	**$D(m^2/sec)$**	**V_0 (m/sec)**
	112671	1.5	0.47	- 2.5
	112838	2.2	0.21	-3.6

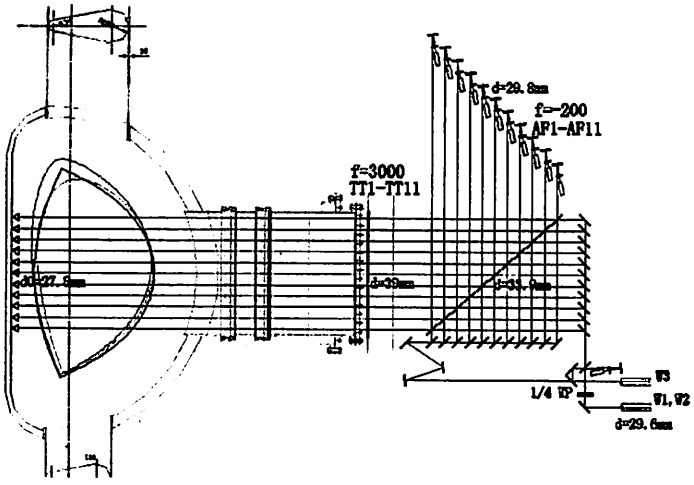

Figure 6 Layout of polarimeter/interferometer on EAST (Liu et al., presentation in QUEST building,2013).

Recently, in particular for fusion, is further amplified by similarities between blobs and ELM filaments, which suggest that the same mechanism is governing their dynamics. To do the comparison studies of blobs in QUEST, HT-7,EAST and ELMy filaments in EAST is approachable way to find their mechanism in near future.

'Blob' type fluctuation in edge plasma, usually observed by some probes or cameras in many devices and configurations. These structures contain excess density and temperature as compared with the background plasma and possibly lead to serious wall erosion, impurity production, heat and particle load, and particle recycling that may become critical for ITER. Recently measurements reveal parallel currents associated with blob-like structures or filaments during ELMs, which result in large net currents to divertor plates. The importance of parallel currents on blob propagation could be inferred by comparing experimental blob speed-versus-size scaling with theory predictions.

Recently, to change the pitch angle (B_z scan, B_t scan) and thus connection length for investigating the blob speed-versus-size scaling and the regime of blob propagating are done on QUEST. Blobs were also was observed in HT-7 and EAST tokamak. To compare the basic parameters (V_b, S_b, statistical information) with different devices and discharge conditions is important for finding the basic principle of blobs. These motivate the development of experiment of blob and dedicated physics study.

In QUEST, to visualize the motion and study the characteristics of blob-filaments, a combination of a fast camera and a movable Langmuir probe were used, as shown in Fig. 7(left). The Langmuir probe can measure simultaneously the ion saturation current, I_s, floating potential, V_f, electron temperature, T_e, and particle flux with a high temporal resolution (1MHz). The K5 camera are typically set on position one (P1) with 40,000 FPS (frame per second) or on position two (P2) with 20000 FPS. On the P1, viewing angle of K5 was about 28° on the mid-plane and the viewing angle was about 60° on the mid-plane on the P2. Two typical images taken by the fast camera are shown in Fig. 1(right), when a blob filament passed through the probe head, the main parameters of blob structures were recorded.

In this blob-filaments experiment, highly reproducible, current-free discharges of Hydrogen plasma are obtained by 2.45 GHz ECRH, with power $P_{RF} \sim 10$ kW. Typical plasma parameters in the edge of plasma are $n_e \sim 10^{16}$–10^{17} m^{-3} and $T_e \sim$ 1–12 eV, with peak values about as twice as higher than the background value. Other relevant parameters are $c_s \sim 10-34 km/s$, $\rho_s \equiv c_s/\omega_{ci} \sim 3-9 mm$ and $\lambda_{mfp}^{ei} \gg \lambda_{mfp}^{en} = o(1)m$, and in this regime the dominant collision channel are Coulomb collisions. The plasma beta is as low as $\beta \sim 10^{-4}$, and the parallel correlation length, L_c, is approximately several meters. Unless we explicitly indicate, any result discussed in the rest of this paper has been obtained in hydrogen plasmas with $B_z \sim 10$ mT, $B_t \sim 40$ mT and radial-scanning measurement by the probe head.

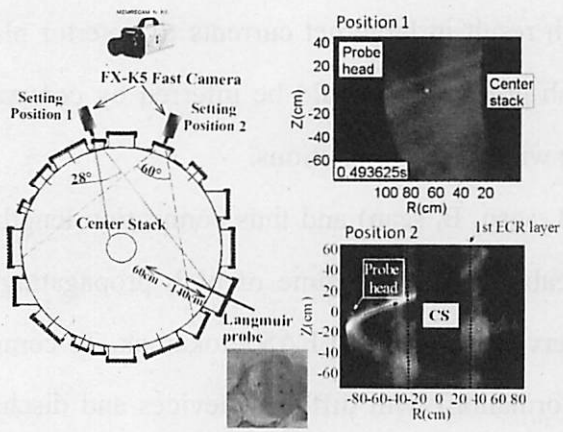

Figure 7 (left) A schematic of combination of the Langmuir probe and the fast camera on QUEST for observing blob-filaments, (right) two typical images, in which the probe head highlighted, are taken from the fast camera on the position one (P1, top) and the position two (P2, bottom).

A simple paradigm for Tokamak SOL was formed to study the effect of radial velocities, and related radial flux of blob-filaments on the midplane of the SOL-like area. The radial velocity of blob was shifted predominantly by the $E \times B$ drift. According to the relation of blob size and the radial velocity, the sheath-connected model has good agreement with the experimental results,as shown in Fig.8. The skewness and kurtosis tend to increase from the source plasma to the first wall, as shown in Fig.9, implying that the density fluctuation at the plasma edge is dominated by the isolated surviving blobs, which can strongly interact with the first wall. This observation also implies that the large amplitude blobs can survive and propagate to the first wall. The larger blob structures, occurring only 10% of the time, can carry more than 60% loss of the entire radial particle flux, as shown in Fig.10. If the particles were confined in the parallel direction, as is the case in tokamaks, blob filaments would constitute the dominant loss channel in the SOL area and strongly interact with the first wall. This can be used as significant references to understand the particle loss in fusion-related experiments such as large magnetic fusion devices.

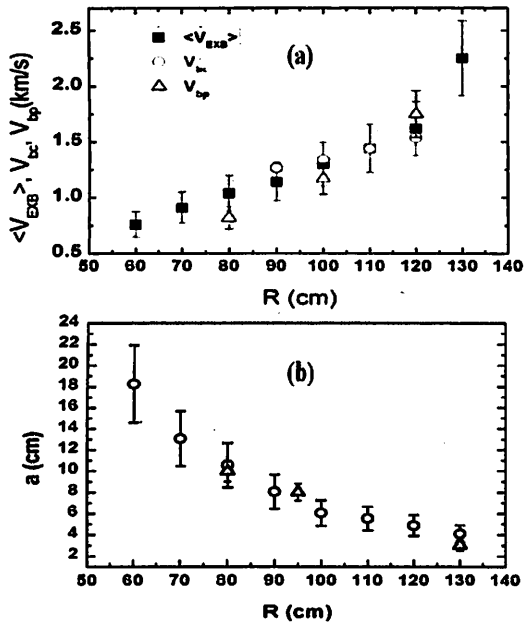

Fig. 8 (a) The radial profiles of $<V_{E\times B}>$ (close square), radial velocity of blob-like structures ,V_{bc}, measured by fast camera images (open circle) ,and V_{bp}, estimated by the time delay of I_s measured with two pins radially separated by 14 mm with probe head. (b) The vertical size of blob structures by sheath connect model in radial probe head scan(open circle) and by fast camera(open triangle). (H.Q. LIU et al.,JNM,2103)

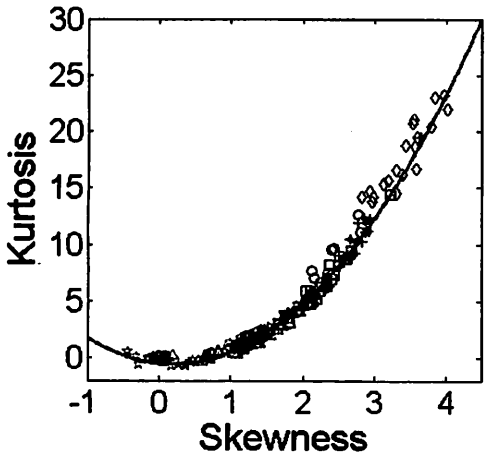

Fig. 9. Kurtosis versus skeness of Is fluctuations. The different marker denote the different discharges, different red markers denote the discharges of the probe radial scan with $B_z/B_t > 0.2$, green and blue

markers denote the discharges with B_z/B_t < 0.1 at R = 100 cm. The all data are fitted by quadratic polynomial (black line), $K = (1.60 \pm 0.27)S^2 - (0.46 \pm 0.20)$ *.(H.Q. LIU et al.,JNM,2103)*

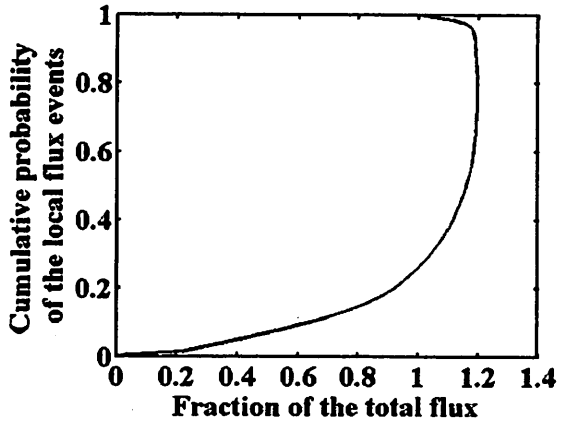

Fig. 10. Cumulative probability of flux events that carry a given fraction of the averaged particle flux.(H.Q. LIU et al.,JNM,2103)

Blobs were investigated in HT-7 tokamak by Langmuir probe. Time-asymmetry of blob structure was revealed with this tool. This time-asymmetry of intermittency may indicate that the spatial shape of blobs may possess a heavy, over-dense front followed by a light tail. Our results show that these radially propagating structures are responsible for much of the total radial transport. In addition, in our experiment it is shown that the blob size, life time and drift velocity have experienced a pronounced change around the shear layer, which may imply that the coherent structures are split by the shear flow. Coherent structures seem to be titled by the developed shear flow in the EXB shear layer, as shown in Fig.11,Fig.12.

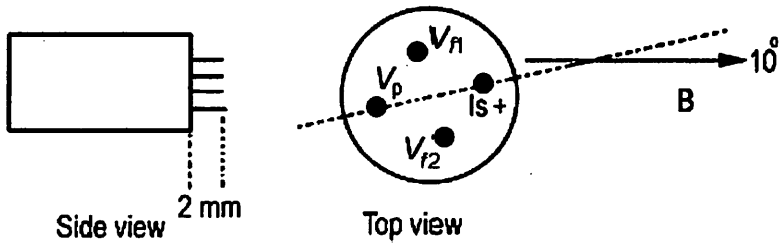

Probe tips Φ 1.0 graphite, 2 mm square array

Fig.11 Layout of Langmuir probe in HT-7 tokamak (N.Yan et al., PST,2010)

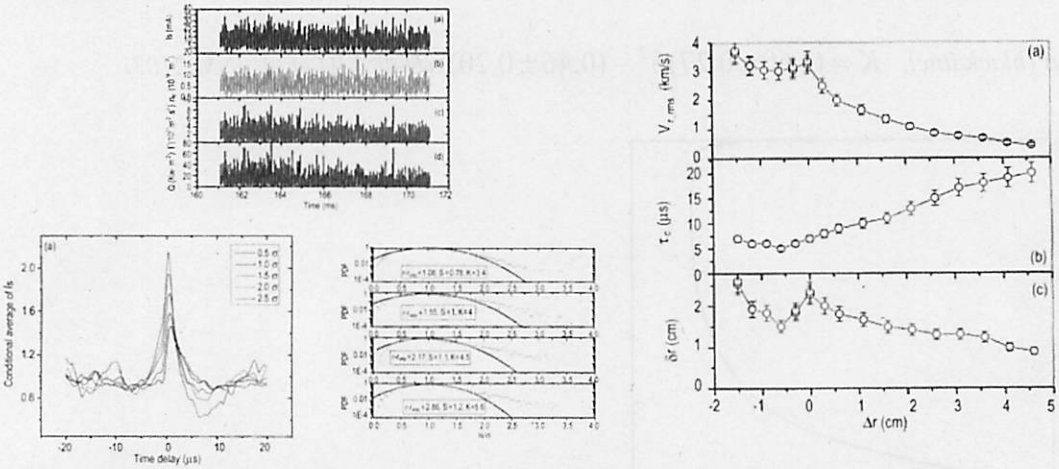

Fig.12 Blobs' results in HT-7(N.Yan et al., PST,2010)

Statistical features of blobs under DN magnetic configuration in EAST were also studied. Both blobs and holes are generated in the shear layer, where shear flow develops. It may imply that the shear flow shears the coherent structure and ejects it as blobs or holes. Blobs propagate from the shear layer to the SOL region, while holes travel in the opposite direction. Their statistical features are quite different. They turn out to be of opposite burst structure, namely blobs are of positive density pulses, whereas holes are of negative. Blobs and hole formed in the steep gradient region of pressure, implying the drift-interchange drive mechanism may play an important role during the formation of blobs and holes, which has been put forward in the simulation research, as shown in Fig.13, Fig. 14.

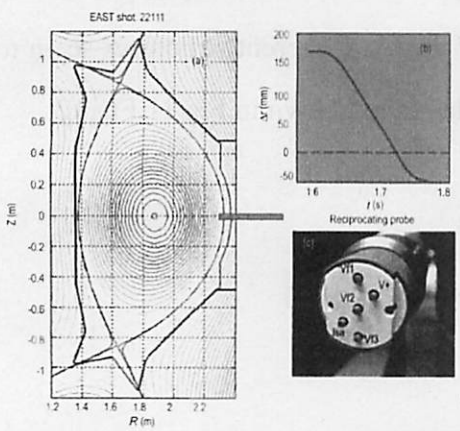

Fig.13 Layout of fast reciprocating Langmuir probe used in the EAST blob experiment(N.Yan et al., PST,2011)

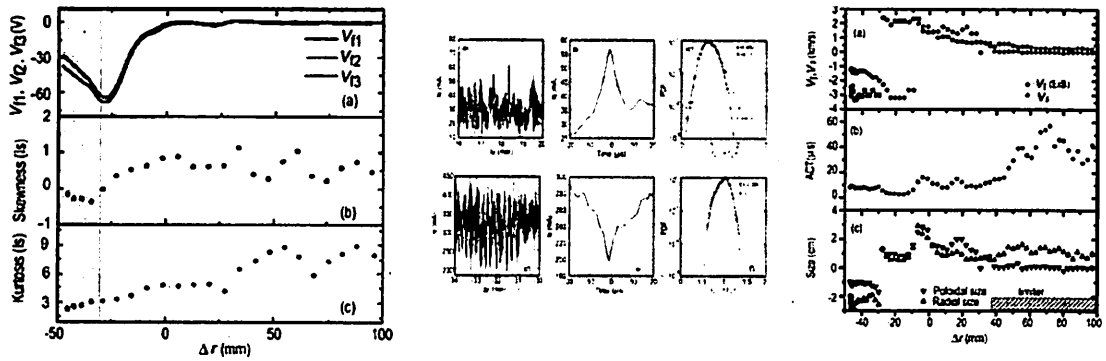

Fig.14 Blobs' results in EAST(N.Yan et al., PST,2011)

Discussions

Steady state operation (SSO) of tokamak plasma is one of the basic requirements for future fusion reactors. QUEST and EAST are both to develop the scientific basis for achieving a steady state condition. Comparative and joint study on QUEST and EAST is most effective thing because the special feature of these two devices (QUEST, SSO with High beta; EAST, SSO with full superconducting coils). All sub-issue studies aim to achieve SSO plasma in QUEST and EAST, and contribute to ITER. Recently, good results were achieved on QUEST and EAST on SSO plasma and have opportunity to challenge for SSO for ITER and future fusion reactors. Exploitation and integration of other plasma physics issues and diagnostic system resources in these two devices and compare the two-side result would have give many fruitful results. Recently, in particular for fusion, is further amplified by similarities between blobs and ELM filaments, which suggest that the same mechanism is governing their dynamics. To do the comparison studies of blobs in QUEST, HT-7,EAST and ELMy filaments in EAST is approachable way to find their mechanism. In these three devices, even if they are in different configurations and sizes, blobs have similar statistical feature. The results may shed light on the physics underlying the formation of blobs. The comparison study in future in these three devices would be energetic way on this issue.

Acknowledgement and comments:

Work supported by the international joint research at the Joint Usage of Research Centers for Applied Mechanics for 2012. We would like to thank our host, Professor K. Hanada, who helps a lot during my staying at QUEST and very appreciate the useful discussions and comments. We also give our thanks to Prof. Zushi, Prof. Nakamura, Mr. Takahashi, Mr. Okina and Mr. Suzukawa, who gave us helpful discussions during our stay in Kyushu University. Our thanks are also expressed to the QUEST group.

It is a good chance for us to join in study in the QUEST. We hope that the international joint research at the Joint Usage of Research Centers for Applied Mechanics could continue to enhance China-Japan cooperation on fusion plasma research in the future.

(Signature)_____

(Name in print) Xiang Gao, Yinxian Jie, Haiqing Liu

国際化推進共同研究概要

No.7

タイトル:Develop and improve EFIT code of the plasma equilibrium reconstruction for SSO operation and advanced physical study on QUEST

研究代表者: Qian, jinping

所内世話人: 花田 和明

来訪期間:

概要:すでに改造が終わっている平衡コードEFITに入力するための2次元X線分布計測装置の準備が終わり、計測を開始した。入力として使えるかどうかをチェックするために3月に来訪予定である。来訪後に改訂した報告書を再度提出の予定である。

RESEARCH REPORT

Date Mar. 23, 2013

Visiting scientists:

(name) Jinping Qian

(position) Associate Professor

(university / institute) Institute of Plasma Physics,
Chinese Academy of Sciences

Host scientist: (name) Kazuaki Hanada

(position) Professor

(university / institute) Kyushu University

Research period: (from) _____ (to) _____

Research subject:

Analysis of Magnetic Measurements Uncertainty in Equilibrium on EAST

1) Summary

The accuracy of equilibrium largely depends on the accuracy of magnetic data. The analysis of uncertainty source shows that each uncertainty source will make a contribution of less than 6G to magnetic probe uncertainty and of 5mWb to flux loop uncertainty on EAST. Uncertainties in PF positions are the largest contributions to both the magnetic probe and flux loops. The overall uncertainty is analyzed based on the statistics over 37 vacuum shots database. The linear and nonlinear uncertainties are about 0.2% and 10mwb for flux loops and 0.6% and 20G for magnetic probes.

Applying overall uncertainty as fitting weight in EFIT, and simulations show the equilibrium uncertainty is 0.5~1.4cm for 6 control gaps, about 1cm for X-points, and 1~1.6cm for strike points (95% confidence) on EAST.

Note that the overall analysis of magnetic measurements uncertainty on QUEST will be performed in the near future.

2) Background

A wide range of uncertainty sources could affect equilibrium reconstruction in Tokamaks: diagnostics active area and position errors, poloidal field (PF) current errors, data integrator-acquisition errors, Noise and others. Whilst in superconducting tokamaks, such as ITER and EAST, the positions PF of coils may have large errors after cooling down. According to the theory estimation, superconducting PF coil position error could lead to an offset of 11G for magnetic probes and 8mwb for flux loops (95% confidence) on EAST, which is the largest contribution to the overall uncertainty for equilibrium reconstruction.

2.1 EAST magnetic diagnostics

EAST is a superconducting device to demonstrate high performance and steady state operation in ITER-like shape with superconducting equilibrium field coils. The design parameters of EAST are major radius R=1.8 m, minor radius a=0.45 m, toroidal field B_T=3.5T, plasma current I_p =1 MA. The EAST magnetic diagnostics are shown in table.1

Table.1 EAST magnetic diagnostics

position	sensor	number	function
Inner	Rogowski loop	3	measurement of plasma toroidal current and plasma control
	Poloidal magnetic probe	3*38	measurement of poloidal magnetic field and equilibrium reconstruction
	Mirnov probe	2*38	measurement of MHD instabilities
	Poloidal flux loop	35	poloidal magnetic flux and equilibrium reconstruction
	Diamagnetic loop	3	measurements of diamagnetic flux, its related to stored energy
	Halo coil	4*8	measurements of halo currents
	Saddle loop	28	measurement of local magnetic flux and locked mode signal
External	Rogowski coil	2*12	measurement of PF coil currents
	Rogowski loop	2	measurement of vacuum vessel current
	Flux loop	5	loop voltage

In these diagnostics, sensors for equilibrium reconstruction contain: one plasma current rogowski loop in vessel, one group of 38 poloidal magnetic probes, 35 poloidal flux loops and one group of 12 PF coil rogowski coils (shown in Fig. 1).

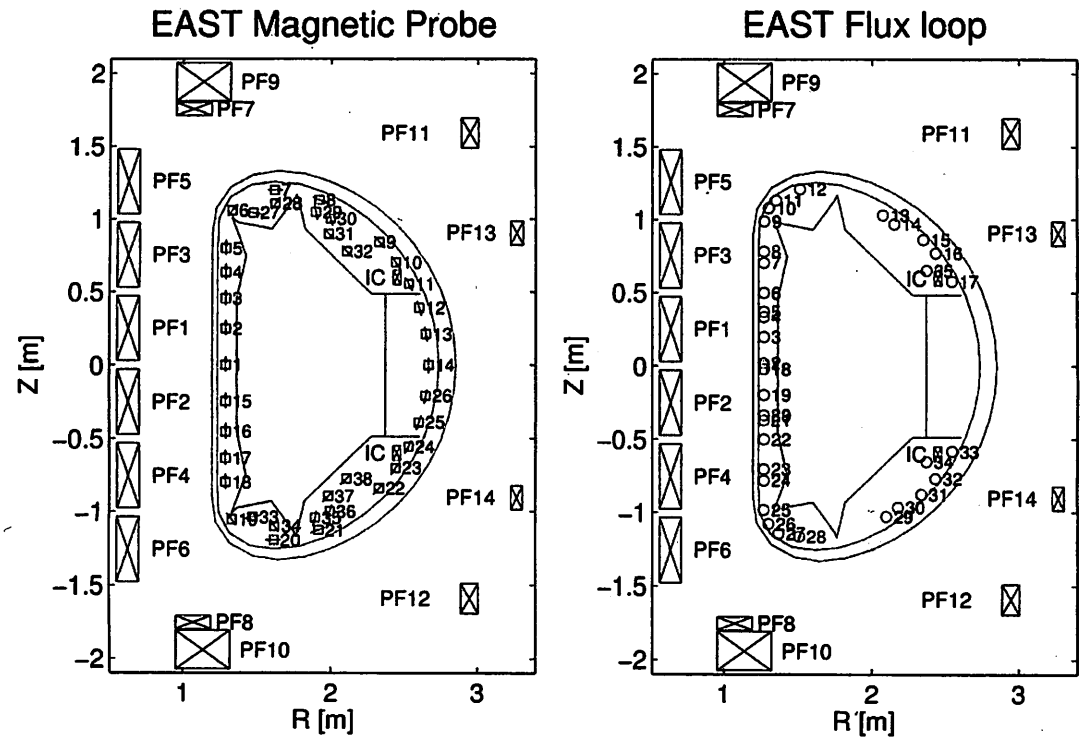

Fig.1 Cross-section of the EAST tokamak, also the distribution of the magnetic diagnostics for equilibrium reconstruction: 14 PF coils (PF 1-14), active feedback coils (IC), limiter (pink lines), flux loops (blue open circle) and magnetic probes (blue open square).

2.2 EAST data integrator-acquisition system

The process to gain integrator information can be summarized by figure 2.

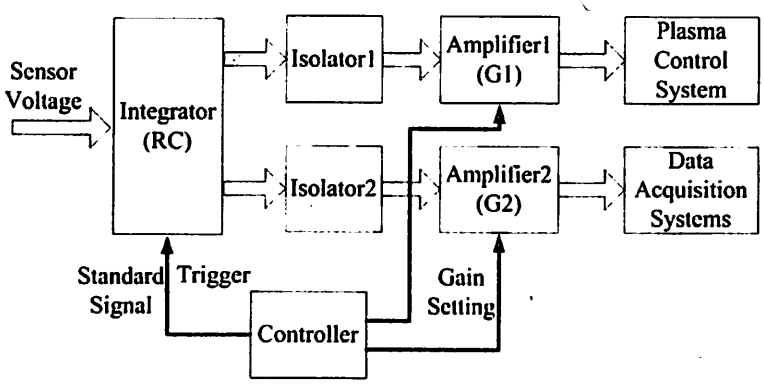

Fig.2 Block diagram of EAST data integrator-acquisition system.

The voltage V_s from a sensor is the time derivative of the magnetic flux linked by the sensor. For a flux loop, $V_s = d\phi / dt$. A signal with value $\frac{G}{RC}\int V_s dt$ is gain by the voltage signal through integrator (RC) and amplifier (G), and when it is acquired by data acquisition system, it should be changed to its origin physics value by a translation coefficient T. The final signal of a flux loop is:

$$\phi = \int V_s dt = \frac{G}{RC}\int V_s dt \cdot T_{fl}$$

Where: ϕ is the measurement result of the flux loop, and G is additional gain of the amplifier, and RC is the time constant of the integrator, and T_{fl} is the translation coefficient of the data acquisition system.

For magnetic probes:

$$B = \frac{1}{NS_{probe}}\int V_s dt = \frac{G}{RC}\int V_s dt \cdot T_{probe}$$

Where: NS is the diagnostics' effective area.

The translation coefficient of the data integrator-acquisition system for magnetic probes (T_{fl}), poloidal magnetic flux loops (T_{probe})are presented as following:

$$\begin{cases} T_{fl} = \dfrac{RC}{G} \\ T_{probe} = \dfrac{1}{NS} \cdot \dfrac{RC}{G} \end{cases}$$

2.3 Process of calibrating magnetic diagnostics system

The calibration of EAST diagnostics can be accomplished by calibration of PF currents, NS values of magnetic probes, and G/RC in data integrator-acquisition system.

The calibrations of PF currents were carried out by two steps—relative calibration and absolute calibration. The 12 Rogowski coils were assembled on one PF transfer line of power supply to gain the relative coefficients by linear least squares fit of measured voltages. And the absolute coefficients were determined by a Hall sensor with an uncertainty of 5‰. The relative and absolute uncertainties of the coefficients are estimated to be 2‰ and 5‰. Only relative uncertainties can affect the results of equilibrium reconstruction.

The magnetic probes' effective areas NS were calibrated in a solenoid coil, driven by a power supply with a few amperes of current at 200 Hz. The calibration reference is a precision-machined standard probe with an uncertainty of 1‰. The reference probe and the aim probe were mounted in the center of the solenoid coil side by side. The effective areas of the aim probes were calculated by comparison of signals of the reference and aim probes. The uncertainty of the calibration is estimated to 5‰.

The integrator–amplifier-digitizer chain parameters G/RC were calibrated by a 3V square-wave power supply at 100 Hz for magnetic probes and 10Hz for flux loops. The values of G/RC were obtained from the slop of the integral triangular wave. The uncertainties of parameters G/RC are 1‰.

2.4 Uncertainty analysis of EAST magnetic diagnostics system

To improve the magnetic diagnostics data, many vacuum shots were carefully designed and performed before each campaign. In all, 37 vacuum shots were used in the analysis, including: individual PF coil powered shots; un-down symmetric PF coils co/counter powered shots; up to 4 PF coils powered together shots. Note that all the PF currents used are 8-9KA/turn.

Sources of magnetic probe or flux loop uncertainty considered in EAST include (shown in table.2): (a) Magnetic probe or flux loop active areas (NS), (b) coefficient of the data integrator-acquisition system (RC/G), (c) magnetic probe position and tilt angle erection error (P_{mp}) or flux loop position erection error (P_{fl}), (d) magnetic probe or flux loop position error from vessel backing deformation(P_{db}), (e) PF coil position (P_{pf}), (f) PF current errors (I_{pf}), (g) signal attenuation of the 70m twisted pair (tp), (h) Noise, (i)

Digitizer bit(bit).

Table.2 uncertainty sources of EAST magnetic diagnostics system

Uncertainty source	uncertainty	
	magnetic probe	magnetic flux loop
NS	5‰	1‰
data integrator-acquisition	1‰	
diagnostics erection error	1mm，0.05°	
diagnostics position errors from vessel backing(50℃)	Data from ref.	
PF coil position	Coil center position error: z 2mm、r 5mm; coil radius error: 2mm	
PF currents	2‰	
70m twisted pair	0.5‰	
Noise	By experiments statistics	
Digitizer bit	0.034G	0.07mWb

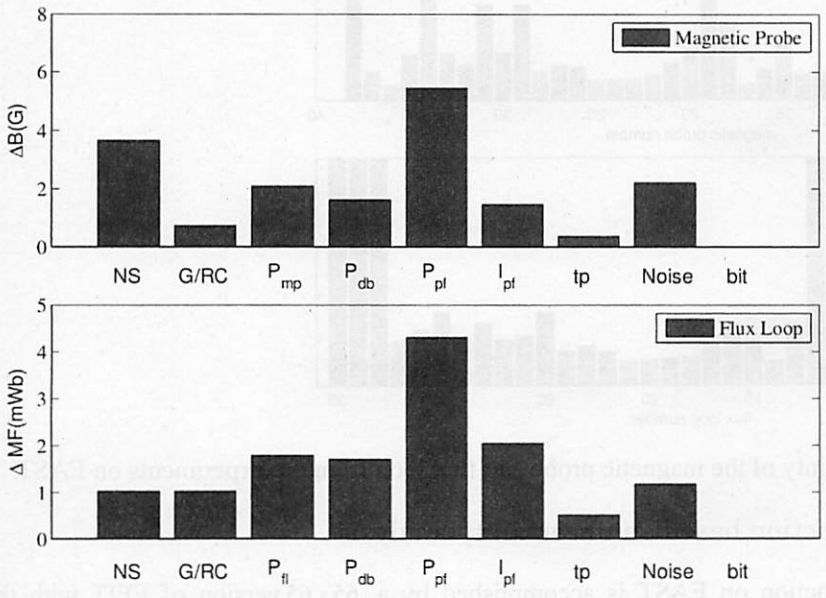

Fig.3 Flux loop and magnetic probe uncertainties of all uncertainty sources

The results of the uncertainty analysis are summarized in Fig.3. Uncertainties in NS and PF coil position are the main contributions to the uncertainty of the magnetic probes; while uncertainties in PF

coil position, flux loop position, PF current and flux loop position errors from vessel backing are the main contributions to the uncertainty of the flux loop. Uncertainties in PF positions are the largest contributions to both the magnetic probe and flux loops, but there is no uncertainty source which contributes the absolutely dominant share.

3. Overall uncertainties based on statistics of experimental data

The overall uncertainty contain linear and non-linear parts. In uncertainty source analysis, the effect of NS and G/RC is classified as linear uncertainty (0.2% for flux loop and 0.6% for magnetic probe), while all effect of the other uncertainty sources is the non-linear uncertainty. The non-linear uncertainty can be gain by statistics of offset from the 37 vacuum shot-database.

Non-linear uncertainty of flux loops and magnetic probes on EAST are shown in Fig.4. The non-linear uncertainties of most of magnetic probe are less than 20G, while non-linear uncertainties of most of flux loops are less than 10mWb. The 6 sensors (pb19, pb38, fl 12, and fl33-35) will not be included in equilibrium reconstruction.

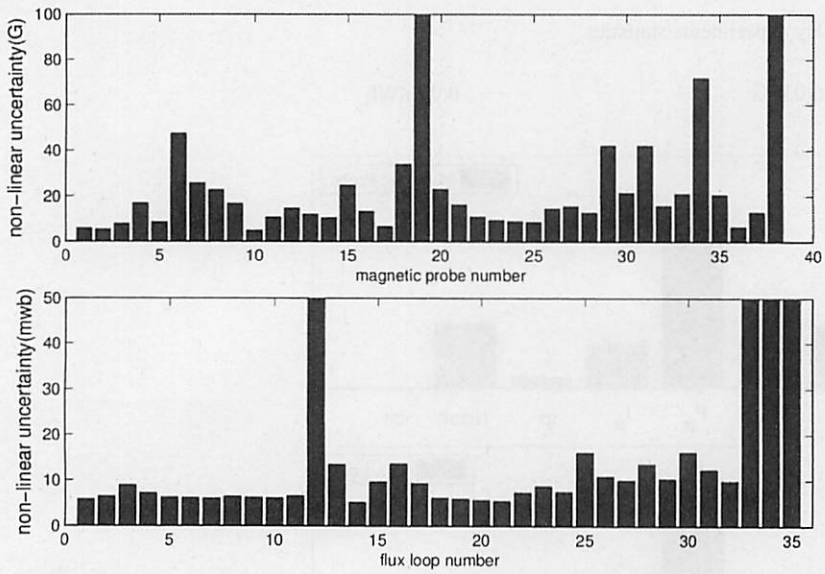

Fig.4 The non-linear uncertainty of the magnetic probe and flux loop from the experiments on EAST.

4. Equilibrium reconstruction based on uncertainty analysis

The equilibrium reconstruction on EAST is accomplished by a 65×65 version of EFIT with the overall uncertainties (see in fig.5).

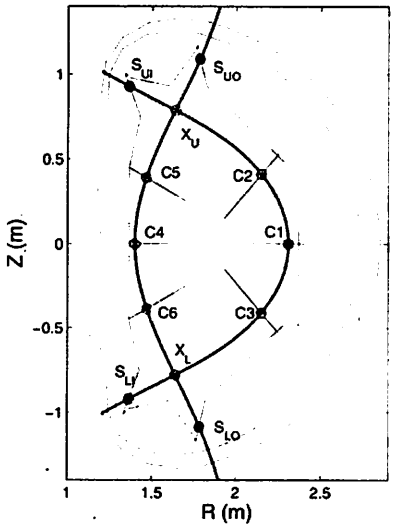

Fig.5 The cross-section of EAST. The green lines, pink lines, the orange lines and the black lines are the vacuum vessel, the limiter, the last close magnetic surface and the SOL control lines separately, and $C_1 \square C_6$, X_U, X_L, S_{UI}, S_{UO}, S_{UI}, S_{LI}, S_{LO}, are 6 control gaps, 2 X-points, and 4 strike point separately.

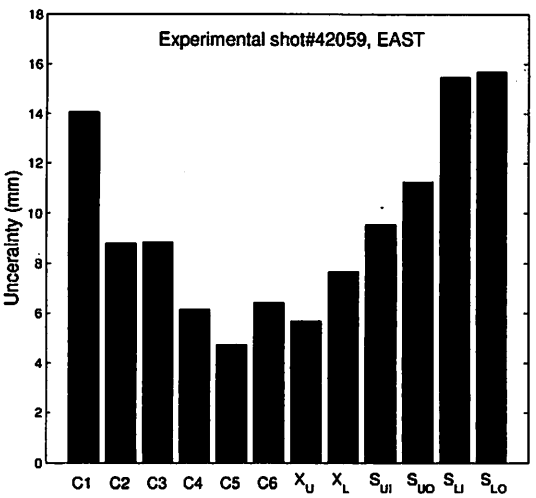

Fig.6 position uncertainties of these 12 points from the equilibrium scan (95% confidence).

The results of the uncertainty of equilibrium reconstruction are summarized in Fig.6. The uncertainties of these 12 points are less than 1.6cm. The uncertainties of the gaps on strong field side and the strike points are larger than others uncertainties. The uncertainty of the gap (C1) is larger due to the farther magnetic sensors located at the low field side.

Jinping Qian

国際化推進共同研究概要

No. 8

タイトル: Collaborative research on QUEST- EBW current drive with divertor, wall and Recycling Control.

研究代表者 : PENG, Yueng-Kay, Martin

所内世話人 :花田 和明

来訪期間 : 2013年2月26日 ～ 3月1日

概要: 2月26日－3月1日の予定で国際WSを開催した。このWSでは質疑の時間を講演時間と同程度に設定し、さらにグループ会議やサマリ報告を行って共通の認識のもとに次期実験や解析について議論した。

Report of workshop on QUEST and related ST RF startup and sustainment research

Kyushu University, February 28 – March 1, 2013

Participants

K. Hanada, Kyushu University
M. Hasegawa, Kyushu University
A. Ishida, Niigata University
T. Maekawa, Kyoto University
K. Nakamura, Kyushu University
Y. Takase, University of Tokyo
N. Tamura, National Institute for Fusion Science
N. Yoshida, Kyushu University
H. Zushi, Kyushu University
H. Idei, Kyushu University

S. Banerjee, Institute for Plasma Research, India; Kyushu University
L. Baylor, Oak Ridge National Laboratory, UT-Battelle, U.S.A.
J. Caughman (teleconference), Oak Ridge National Laboratory, UT-Battelle, U.S.A.
S. Diem (teleconference), Oak Ridge National Laboratory, UT-Battelle, U.S.A.
M. Peng, Oak Ridge National Laboratory, UT-Battelle, U.S.A.
V. Shevchenko, Culham Center for Fusion Energy, U.K.

Introduction

A workshop dedicated to the subject of radiofrequency (RF) startup and sustainment plasma research on QUEST and related spherical tokamak (ST) experiments in Japan and U.K., was held at the Research Institute of Applied Mechanics (RIAM), Kyushu University during February 26 – March 1, 2013. The workshop was attended by twenty-five research leaders, researchers, and graduate students, from Kyushu University, the University of Tokyo, Kyoto University, National Institute of Plasma Science, Niigata University, Oak Ridge National Laboratory (ORNL, U.S.A.), and Culham Center for Fusion Science (CCFE, U.K.) attended.

RF plasma startup and sustainment, including sustained plasma-wall interactions, is a remaining research gap to be filled to realize compact, cost-reduced ST fusion energy applications.

Eighteen presentations were made and were accompanied with extensive discussions. The participants obtained substantive common understanding of the key scientific and technical research issues of interest, and developed recommendations of the next research steps to take to resolve these issues.

The following summarized the results of this workshop, organized as follows:

Overall workshop summary

1) Formation of closed flux surface (CFS) via RF driven electrons,
2) Evolution of electron distribution function in phase space,
3) Development of optimal startup scenarios
4) RF plasma wave physics and wave launching,
5) Creation of multi-keV H^+ or H^0,
6) Improved particle pumping and pellet fueling,
7) MHD equilibrium modeling in presence of confined energetic electrons, and
8) Importance of plasma rotation and ExB shear.
9) Cross-machine comparisons and diagnostic needs

Overall Workshop Summary

- Steady progress has been obtained in the conditions of RF-driven and sustained plasmas on QUEST, LATE, TST-2 in Japan, and MAST in U.K. Without or with only a transient blip of solenoid induction, plasma currents per input RF power have reached 0.2 – 0.5 A/W. Though the total plasma current achieved so far were limited to the range of 15 – 45 kA, the plasma regime was characterized by ~keV to 100's keV in electron temperature (Te), up to 30 s in sustained duration, ~1017 – 1019 /m3 in density. Such high Te's speak well for research toward >100 kA current in the next experiments via increased RF power and improved plasma fueling and wall control.
- Improvements in understanding of the key physics processes, and next research steps were obtained on the following topics :
    1) Formation of closed flux surface (CFS) via RF driven electrons,
    2) Evolution of electron distribution function in phase space,
    3) Development of optimal startup scenarios
    4) RF plasma wave physics and wave launching,
    5) Creation of multi-keV H^+ or H^0,
    6) Improved particle pumping and pellet fueling,
    7) MHD equilibrium modeling in presence of confined energetic electrons,
    8) Importance of plasma rotation and ExB shear, and
    9) Cross machine comparison and diagnostic needs.
- The participants of the workshop recommended conducting cross-machine comparisons via:
    1) Coordinated experiments and data analyses, utilizing varied capabilities among different research groups in RF systems, plasma parameters, diagnostics, and modeling tools.
    2) Sharing of unique resources (personnel, equipment, analysis tools), and increasing the level of coordination of research planning.
    3) Enhanced bi-lateral and multi-lateral collaborations among QUEST, LATE, TST-2, and MAST.
- The results of these enhanced efforts among the ST research community will be the subject of the next workshop to be planned in February 2014.

1) CFS formation via RF-driven electrons

In finite temperature plasmas immersed in a toroidal field Bt (counterclockwise when viewed from top), the electrons drift downward while the ions drift upward due to the field gradient and curvature. The electrons reach and enter the bottom wall while the ions reach the top wall and recombine with the electrons. This results in a upward current Jv in the plasma that is returned through the conducting vessel. A downward directed vertical electric field Ev within the vessel is thus created due to the charge accumulation to maintain a voltage against the vessel current times the vessel resistance. Ev x Bt drift of the ions and electrons points radially outward, requiring a balancing force to maintain the radial location of the drifting electrons and ions within the vessel.

When a negative (pointing down) vertical field Bv is introduced, helical field lines are created to provide a parallel path for the internal electron circulation to form a toroidal plasma current loop. Let us consider the problem in terms of the radial force balance of this plasma loop. First, toroidal plasmas have finite pressure and tend to expand horizontally by the ballooning effect. Therefore, there must be a balancing force to this expansion. A balancing force is generated by the interaction with the toroidal field (Jv x Bt). In addition, the helical field provides a parallel path that connects the top and the bottom of the vessel. The presence of Ev causes a toroidal current Jt (counter clockwise when view from top) that equals to the plasma conductivity (η) and the parallel projection of the Ev (Ev x Bv / Bt) divided by the connection length (L = H x Bt / Bv). This results in a radially inward Jt x Bv and provides another balancing force. Both currents originate from the thermal energy of electrons, which is provided by RF heating.

An increasing electron temperature Te increases η and Ev, which in turn increase Jt. The inward force of Jt x Bv dominates over the other inward force of Jv x Bt. This Jt increases further with the increased bulk electron pressure Pe (= ne x Te), and eventually the self vertical field from Jt almost cancels out the external field Bv at the inboard side of the current channel. At this moment a significant forward portion in electron velocity space (in the direction of the toroidal plasma current) gains

1) CFS formation via RF-driven electrons - continued

confined orbits in physical space. As a result, the forward energetic electrons can for the first time accumulate in this area of the velocity space and gain further energy and density, generating large additional toroidal current [1]. This additional current closes additional field lines on the inboard side of the current channel, expanding the cross section of the closed flux surfaces (CFS's).

This process of forming closed flux surfaces appears to be consistent with the plethora of observations of RF-driven plasma startup experiments so far. Successful startup has been shown to depend on a number of operational conditions and scenarios, including Bv evolution and decay index (radial profile), the size scale (major radius), the aspect ratio of, the magnitude of Bt, the initial gas pressure, wall conditions, and the available rf power Prf, etc.

An important goal of research is therefore to increase Pe in open field configurations and ensure a smooth transition to the expanding CFS's. For example, an positive decay index of Bv creates a Bv mirror that improves confinement of the forward trapped electron orbits at higher energies than the thermal electrons. These trapped electrons absorb ECH wave energy effectively, particularly where the RF electron resonances are located near the banana tips of the trapped energetic electrons, where the electron dwell time is maximized. These electrons generate toroidal current via orbit precession, which increases with increasing energy and density of these electrons in a regime of low collisionality. These electrons in turn deliver energy to the colder bulk electrons via collisions.

At present the prescriptions are uncertain, given R, aspect ratio, Prf, Bt, and resonance locations, regarding the best experimental operation scenario to control Bv, particle fueling, and wall conditioning to achieve a smooth transition to maximum driven current. Experiments including TST-2, LATE, QUEST, MAST, SUNIST, DIII-D, JT-60U, KSTAR, etc., have tested various scenarios by trial and error over wide parameter space . It may be useful to jointly examine these experimental results, update the modeling for the CFS formation, to design the next step startup experiments.

[1] T. Maekawa et al. Nuclear Fusion **52** (2012) 083008.

2) Evolution of electron distribution function in phase space

Issue: Improve the energetic electron energy and orbit, as the absorbed RF power is lost primarily via orbit loss of these electrons, leading to large deposition on and out-gassing from the plasma facing component (PFC) that can adversely affect the RF-driven startup process.
Recommendation: Obtain detailed understanding of the birth and loss mechanisms of the confined energetic electrons, and their distribution function in space and velocity. Diagnostics for such information should be developed and implemented. A critically important research goal is to develop an RF-driven plasma start-up and sustainment modeling / simulation tools that integrates key physics mechanisms covering a variety of phenomena of interest, as discussed below.
Discussion: In quasi-steady state condition for time scales long compared to the electron kinetic interactions, guiding-center orbits of electrons that intercept a given mid-plane location (Rmid) of a toroidal plasma with up-down symmetry, can be parameterized in such constant of motion parameters as (E,L,m) representing (energy, angular momentum, magnetic moment). A successfully RF-sustained plasma should contain copious energetic electrons with confined orbits, filling a sizeable volume in this phase space. RF-heating of the confined electrons diffuses the electrons toward higher parameters in this space. In the absence of collisions and radiative energy loss (such as via Bremsstrahlung), this process would move these electrons into lost-orbits.

The confined electrons can also be lost through large pitch-angle scattering by collisions with ions or other, particularly colder, electrons into the lost-orbit region of this phase space. This is consistent with the observed negative impact of high neutral pressure on the startup plasma, introducing copious cold electrons in the presence of confined energetic electrons. These collisions also cause large energy exchange, dramatically reducing the energy containment time. Non-axisymmetric field components, such as toroidal field ripples, magnet field errors, eddy current fields induced by global MHD instabilities, and even plasma transport inducing fluctuations, can introduce additional more refined orbit loss mechanism.

2) Evolution of electron distribution function in phase space – continued

The lost electrons so introduced are distributed non-uniformly in this phase space, leading to non-uniform distribution of impact locations on the plasma facing components (PFCs).

The distribution function of the confined electrons depends on the low temperature source located near the "origin" of the phase space, and the diffusion drivers, such as the RF power density, the locations of RF resonance layers, N||, and the ECW/EBW ray trajectories. These in turn depend on the toroidal plasma equilibrium configuration and profiles. The presence of large plasma potential improves orbit confinement, particularly for colder electrons and ions.

Modeling and simulation of the electron confinement and transport in phase space is required to understanding this complex topic.

Bi-Maxwellian like distribution function was obserbed.

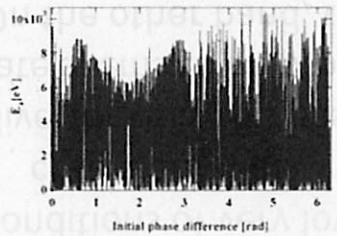

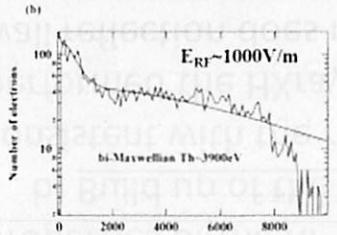

Calculation of 5×10^6 cyclotron periods (~ 600μsec) was executed, and bi-Maxwell type of distribution function appears. Thermal temperature is about 4keV, which corresponds to observed temperature od energetic electrons.

$$W_{RF} = \sqrt{\frac{\varepsilon_0}{\mu_0}} E_0^2 S$$

$\varepsilon_0 = 8.854\times10^{-12}$ [F/m]
$\mu_0 = 4\pi\times10^{-7}$ [H/m]
$E_0 = 1000$ [V/m]
S=5.6[m2]

W_{RF}~15kW

Production of energetic electrons

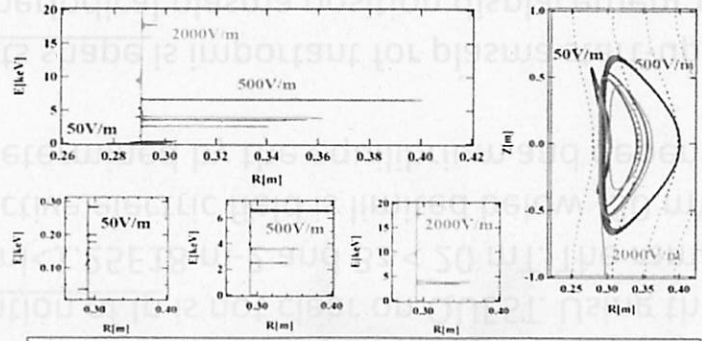

Orbit calcultion including RF acceleration are executed. Several keV electrons was observed even in a banana orbit.

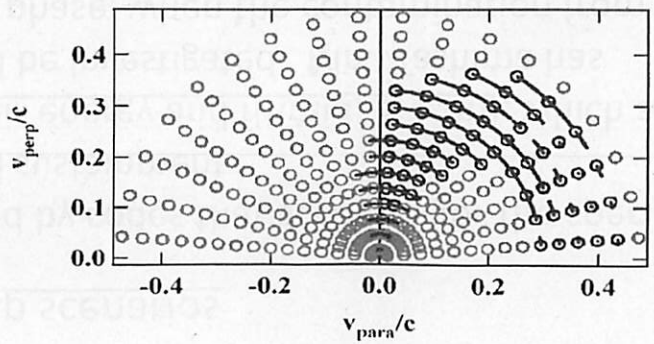

3) Optimizing startup scenarios

a) Improved reconstruction of flux surfaces followed by codes that accounts for the special properties of the RF-driven plasma during startup and sustainment.

b) Build up of the fast electrons with respect to their energy and f(Rmid, E, L, m), which are consistent with the reconstructed flux surfaces should be investigated. Mrs. Tashima has performed the HXray measurements in the very early phase, when the contamination from the wall reflection does not seem to play an important role on co/ctr measurements under the conditions of very low power and low plasma current.

c) A relation between the ramp-up rate and saturation of Ip is not clear on QUEST. Using the divertor coils this has been studied with Prf<150kW, nl<1.25E18 m-2 and Bz < 20 mT. The ramp-up rate seems to be proportional to Prf/nl, and the inductive electric field is limited below -30 mV/m. On the other hand, the maximum current is mainly determined by the equilibrium and depends on the Bz.

d) The real-time control of a plasma position and its shape is important for plasma start-up and the steady state plasma sustainment. For instance a periodical plasma position displacement may be required for the steady state discharge in order to avoid a local heat load to the strike point. Further, the plasma start-up phase depends on several factors such as the wall condition, initial neutral gas pressure, vertical magnetic fields configuration, and its time variation. During plasma start-up, whereas the controls of plasma position and its shape are required, the open field currents play important roles [1, 2]. Although the reconstruction of the plasma current profile are proposed [2 - 4], that for real-time plasma shape with open magnetic field area is still to be developed.

[1] Ejiri, et al., Nucl. Fusion, Vol. 49, 065010 (2009)
[2] A. Ejiri, et al, Nucl. Fusion, Vol. 46, pp. 709-713 (2006)
[3] Y. S. Hwang, et al., Rev. Sci. Instrum., Vol. 63, No. 10, pp. 4747-4749 (1992)
[4] T. Yoshinaga, et al., Nucl. Fusion, Vol. 47, pp. 210–216 (2007)

3) Optimizing startup scenarios – continued

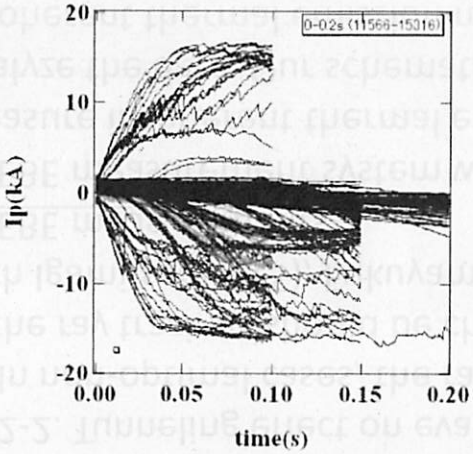

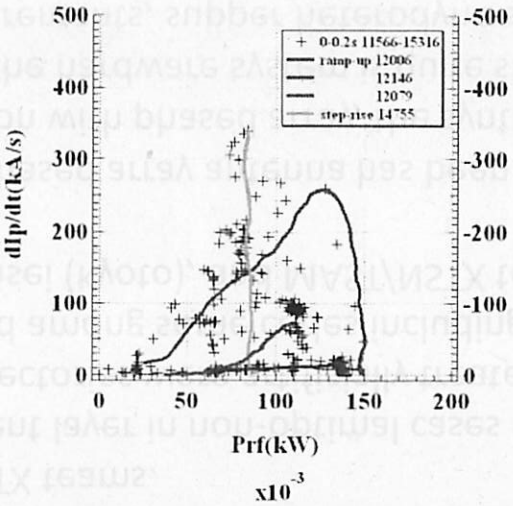

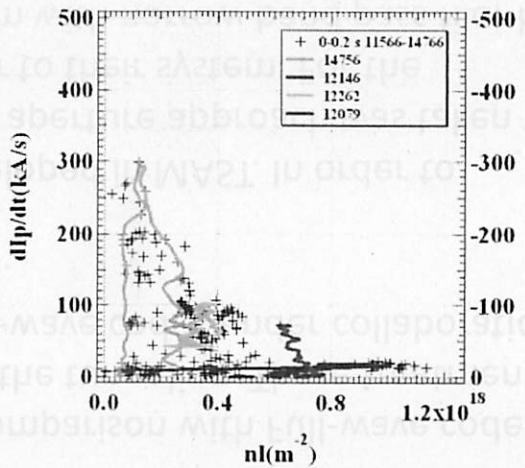

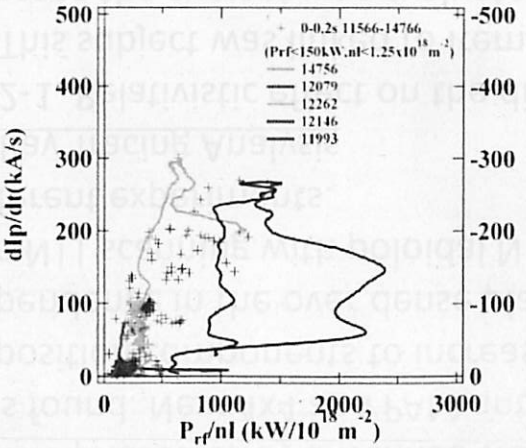

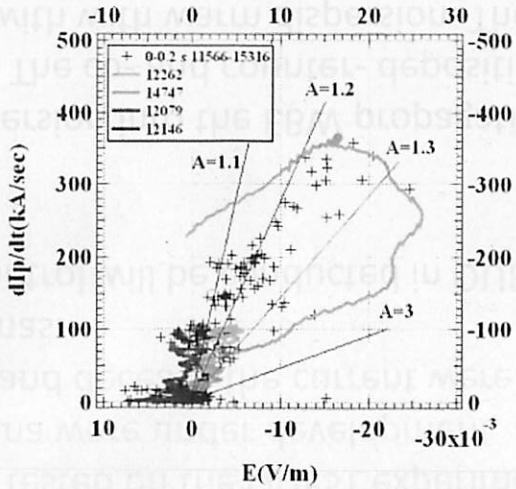

4) RF plasma wave physics and wave launching

1. Experiments: N||-dependence of CD with Phased-array Antenna

The phased array antennae were tested on the QUEST experiments. No clear dependences on N|| was found. New 4x4 and PAM antenna were under development, and will be used. The co- and counter-deposition components to increase and decease the current were one of candidates for unclear N|| dependence in the over dense plasmas.

The N|| scanning with poloidal N control will be conducted in QUEST, and should be compared to the different experiments.

2. Ray Tracing Analysis

2-1. Relativistic effect on the dispersion into the EBW propagation

This subject was linked to Item 1. The co- and counter- deposition components to increase and decease the current was evaluated with with warm dispersion. The relativistic dispersion will be used under collaboration with MAST/NSTX teams.

2-2. Tunneling effect on evanescent layer in non-optimal cases (in comparison with Full-wave codes)

In non-optimal cases, the ray trajectories were artificially treated in the tunneling. These treatments in the ray tracings should be checked among some codes including Full-wave codes under collaboration with Igami-san(NIFS), Fukuyama-sensei (Kyoto), and MAST/NSTX teams.

3. EBE measurements

EBE measurement system with phased array antenna has been developed in MAST. In order to measure incoherent thermal emission with phased array, the synthetic aperture approach was taken to analyze the data. Our schematic of the hardware system is quite similar to their system. For the incoherent thermal emission measurements, supper heterodyne system with narrow band pass filer has been prepared. The incoherent thermal emission was correctly measured in the test stand. The synthetic aperture approach and frequency selection approach with the narrow band pass filter will be compared.

4) RF plasma wave physics and wave launching - continued

4. Wave polarization and nonlinear wave mechanisms

The role of wave polarization and wave type for plasma start-up remains an open question. For experiments on MAST, the frequency of the wave (28 Ghz) is above the cut-off frequency during start-up. For some of the other machines that use 2.45 Ghz, the wave frequency is below the cut-off frequency. On MAST, how much of the launched O-mode gets absorbed at the EC layer before it hits the center post, where it gets converted to X-mode. What other role does the O-mode have?

It is demonstrated that large diameter waveguide can be used to deliver RF power that is efficiently absorbed by the startup plasma. In such cases, is the RF-plasma mechanism limited to EBW or can it also be whistler waves that bounce off the off the center stack and propagate from the high-field to the low-field region before they get absorbed?

5) Creation of multi-keV H^+ or H^0

Examination of SS, Mo, and W in-vessel coupons from recent experimental campaigns on QUEST revealed copious dislocation loops likely due to impacts of multi-keV H^+ or H^0. Discussion during the workshop identified several possible mechanisms for the production of such ions that will require additional measurements and modeling to resolve:

1) Parametric decay of ECW/EBW to LHW that can directly heat protons via Landau damping. This suggests measurement of RF side bands in vessel.
2) Presence of positive, multi-keV plasma potential between the LCFS and wall. This suggests measurement of space potential in vessel, such as via heavy ion beam probe (HIBP) or Stark-effect radiation line splitting spectroscopy.
3) Heating via electron collision of cold ions initially confined within the LCFS before guiding center orbit loss of these heated ions. This suggests such as deep fueling and low-Z impurity seeding within LCFS to enable radiation line spectroscopy to diagnose Ti and ion flow and ExB. (See #6.)

Multi-keV H^0 could then be produced from H^+ via charge-exchange with cold H^0, which in turn includes the 3-eV Frank-Condon H^0 resulting from the dissociation of H_2 desorbed from the wall. Aside from active gas fueling control, desorption from wall during incident plasma electron and photon fluxes can be the primary source. In the case of starting plasma within a clean cold metallic wall, monolayers of H^0 first accumulate on surface resulting in large wall pumping. This progressively increases the rate of desorbed H^0 and H_2. The desorption rate then increases rapidly when the wall temperature increases and introduces additional particle source via diffusion from the material bulk, leading to net large wall fueling. This transition in fueling source from gas puff against strong wall pumping to uncontrolled wall fueling has causes difficulties in plasma density control. To improve fueling and density control over long durations and ensure reproducible plasma conditions,

4) hot walls of W or other high temperature tolerant materials with low H solubility should be used for longer plasma durations than cold metallic wall particle and temperature evolution times.

6) Improved particle pumping and pellet fueling

It has been observed that high neutral pressure hampers the startup plasma. Use of hot walls are planned to control and limit the neutral pressure near the edge of the energetic electron cloud, which extends beyond the CFS by ~10cm in the case of QUEST.

A proposal was made to inject particles (TESPEL - NIFS, H2 pellet) deeper into the CFS region of the plasma generated by RF current drive when and if edge fueling is prevented by use of hot walls.

Pellets further can provide a fast electron diagnostic since the pellet ablation is strongly affected by fast electrons. Such a tool could provide needed data on the fast electron distribution in the plasma cross section using appropriate pellet ablation diagnostics. Camera imaging would be the most useful way to utilize this concept, but fixed photodiode arrays can also be useful.

Pellet fueling to increase the ion density can utilize the favorable inner launch geometry afforded by the ST geometry. Experiments on tokamaks and MAST have shown that the pellet ablation induced ExB drift plays a strong role in deep pellet deposition when pellets are injected from the high field side. This technique requires good port access that is available on QUEST. A system with curved guide tubes can be used without having to move and injector to different ports of the machine.

Pellet ablation can be used also as a diagnostic to determine local field line pitch angle in the confined plasma region. This requires imaging of the pellet ablation cloud with good spatial resolution. This technique can be useful when substantial Ip and Bv are established.

Optimized pumping geometry is critical for long pulse particle control in fusion devices. For the ST this means that the divertor strike point should be near pumping ducts to obtain high neutrals ballistic conductance to pump inlets. The pumping on QUEST can benefit from an optimized geometry that also prevents the RF power from reaching the cryopumps.

TESPEL offers the added capability to deposit minute amounts of low-Z impurities into the CFS region of the startup plasma. The ensuing evolution of line radiation from these impurities afford opportunities to diagnose the ion confinement conditions of the CFS plasmas.

7) MHD equilibrium with energetic electrons

In normal aspect ratio tokamak of low beta, the plasma shape can be reconstructed by FCA (Filament Current Approximation) with adequate precision. In case of RF-driven ST plasma, plasma current is shifted outward via the energetic electrons. Therefore, several methods have been proposed to reconstruct such plasma equilibria with large currents from energetic electrons. It is necessary to use different approaches to address varied physics issues, and compare these approaches when applied to common issues.

Presently the following approaches are being developed and used:

1) E-FIT code: The standard version can fit the magnetic data to reconstruct the isotropic-pressure equilibrium. An improved version is needed to accommodate plasma current in the open magnetic field line region surrounding the CFS.
2) Maekawa code: This code takes into account the effect of anisotropic plasma pressure.
3) Ishida code: This code calculates two-fluid plasma equilibrium with different Te and Ti, large plasma flow, and the associated electric field.
4) Ejiri code: This code adopts truncated surface function about the current density in open magnetic field region.
5) Hasegawa code: The current density profile is approximated by a distribution of current filaments.
6) CCS code: This code can reconstruct plasma shape using the magnetic flux loop data, without relying on the interior profile and anisotropy of the plasma pressure.

Now various plasmas are analyzed by codes available in the laboratory, where the plasma was obtained. It is recommended that representative plasma data be made available for analysis and comparison using the above listed equilibrium reconstruction codes.

8) Importance of plasma rotation and **E** x **B** shear

Plasma rotation (both toroidal and poloidal) is believed to play a vital role in the regulation of instabilities since it can alter the **E** x **B** shear profile. It is now well known that radial shear in poloidal rotation can suppress turbulence and allow improvement in energy confinement. Thus, experimental and theoretical investigation of the poloidal rotation is of particular interest as it can provide an effective tool towards advanced tokamak operation in spherical tokamak.

Plasma rotation has been studied thoroughly with external momentum input like NBI and also with RF waves like ICRH and IBW. However, experimental observation of plasma rotation induced by ECRH/EBW without any external momentum input is still not reported. As spherical tokamaks mainly rely on non-inductive current drives, it could be an added feature if ECW induced poloidal rotation can be demonstrated. Theory suggests that it is possible with ECW through pump-out of resonant electrons. Experiments are being attempted in this direction on QUEST and may be taken up in other toroidal devices as well. If the role of ECW, which is fairly commonplace nowadays on plasma devices, is established in generating plasma rotation, it could provide an excellent option towards better sustainment of RF plasmas.

The necessary tasks could be as follows:

1) This effect has been observed recently in QUEST. But, it is still not reported in other tokamaks and spherical tokamaks. So, it will be good to do a multi-machine comparison by designing suitable experiments and diagnostics.
2) Conventional diagnostic techniques like probes may not suffice in dealing with energetic electrons. So, non-intrusive techniques like fast visible imaging, ECE imaging, BES imaging etc. can be tried on to measure the flow and associated components of the electric field.
3) Such rotation may enhance mechanisms that can generate poloidally asymmetric particle profile/source. So, measurement of the flow with shallow pellet injection and gas puffs can also be attempted to prove the principle.

9) Cross-machine comparisons and diagnostic needs

1. Cross-machine start-up comparison

1.1. Cross-machine comparison in the case of RF - plasma interaction in the EC range.

It is important to identify EC harmonic where interaction is predominant. Also the plasma entrance into the overdense regime with large Wpe/Wce must be identified. This is due to the drastic differences in the mechanisms of plasma-wave interaction, excitation, and absorption of EBW are totally different from the electromagnetic interactions of the EC harmonics. The electromagnetic-EBW mode coupling and propagation also depends strongly on the ratio Wpe/Wce. It is further possible that mode conversion to lower hybrid occurs during the diffuse lower density stage of plasma initiation.

1.2. Comparison of data from different machines must include most important dimensional and dimensionless scales or ratios. For example, the scales responsible for the mode coupling must be identified. Density scale length to vacuum wavelength ratio, plasma size to vacuum wavelength ratio, etc. should be included. Due to the wide parameter space covered by the experiments, it is necessary to clarify the differences between quasi-optical and optical propagations of waves.

1.3. Comparison of current generation efficiency can be reduced to some universal parameters . This can be represented by a figure of merit F: I = F *Prf*Te/Ne, or Te/Ne ratio can be included into efficiency E providing normalization: I = E*Prf

1.4. It is important to obtain detailed measurements of the electron distribution function f(v) over a wide range of energy/pitch angle. Diagnostic approaches for this purpose include Thomson scattering for colder bulk plasma (~keV), hard X-ray spectroscopy for high energy electrons (100's keV), and new diagnostics for intermediate energies (10's keV) still to be developed.

9) Cross-machine comparisons and diagnostic needs - continued

2. Critical questions for RF start-up understanding

2.1. What is the effect of initial N|| on EBW start-up?

Extensive EBW ray-tracing modeling of MAST, NSTX, GLOBUS, PEGASUS and other ST plasmas show strong dependence of EBW propagation on poloidal magnetic field curvature and sensitivity to small changes in the initial N|| values. These differences lead to opposite CD directions for EBW launched above and below the midplane. EBW experiments on COMPASS-D and MAST confirmed these predictions. Experimental results from LATE and QUEST appear not to encountered these phenomena, as no asymmetry between above and below midplane wave-plasma interaction was observed. The causes for this difference will depend on the answers to the following questions:

* Is it a result of different degree of plasma overdense?
* Is it a result of different dimensional scales?
* Is EBW propagation involved in the process?

It is important therefore to design special experiments among different machines to answer these questions.

2.2 EBW ray-tracing simulations for QUEST plasma presented at WS showed N|| can be >> 1 in the absorption zone. This could be a result of using 'warm' dispersion relation for EBW propagation. It was found at Culham that relativistic effects have strong influence on EBW propagation and damping even at relatively low temperatures <100eV. Relativistic dispersion leads to larger Doppler broadening of EC resonances and EBW absorption with N|| ~ 1 in the absorbing layer. It is suggested that the available ray-tracing codes from various research institutions be benchmarked by modeling the same sets of experimental conditions from different experiments. The outcomes of the modeling comparisons can be used to design experimental tests on appropriate machines for resolution.

国際化推進共同研究概要

No.9

タイトル: Feasibility study for solenoid-less plasma start-up capability in quest using transient coaxial helicity injection.

研究代表者 : RAMAN, Roger

所内世話人 :花田 和明

実施期間 : 2013年1月17日 ～ 1月30日

概要: 同軸ヘリシティ入射の実験を行うためのデザインを終了した。電極の形状、絶縁物の材質や構造等について詳細に検討し、結果としてデザインは図面化され、現在製作の見積もりを依頼中である。見積金額を受けてこの実験を実施するための予算申請を日米双方で行うこととした。
結果は来年度、明確になるが、この共同研究のおかげでデザインが確定したことは大きな成果である。Raman 氏はこのデザインの結果を論文投稿する予定である。

Proposal for Implementing CHI capability on QUEST *
26 March 2013

R. Raman[1], T.R. Jarboe[1], M. Ono[2], K. Hanada[3], B.A. Nelson[1], M. Nagata[4]
[1] University of Washington, Seattle, WA, USA
[2] Princeton Plasma Physics Laboratory, Princeton, NJ, USA
[3] Kyushu University, Kyushu, Japan
[4] University of Hyogo, Himeji, Japan

This proposal is for a US-Japan collaborative research between Kyushu University and the University of Washington for implementing Coaxial Helicity Injection (CHI) capability in the QUEST Spherical Torus at Kyushu University. This report is an update to the previous report dated 27 March 2012. Therefore, information from the previous report is only mentioned briefly, so as to make this report easier to read. The power supply parameters are not repeated here as they are described in the previous report.

On QUEST, CHI is capable of contributing towards multiple roles. These include: (1) Solenoid-free plasma start-up: CHI can generate significant amounts of non-inductively generated closed flux plasma current through the process of *transient* CHI. (2) Edge biasing: By driving few kA of current along the outer scrape-off-layer (SOL), it provides a means to inject density along the SOL and thereby increase the edge density and vary the density gradient near the separatrix region in support of EBW current drive studies. (3) Steady-state current drive: By continuously driving current along the scrape-off-layer, it offers the possibility of continuous current drive to modify the edge current profile. The all-metal nature of QUEST in addition to its capability for 400 kW of ECH power would both reduce the amount of low-Z impurities initially injected during the application of CHI and because of its ECH heating capability allow a relatively greater fraction of the injected low-Z impurities to burn through radiation barriers, which is necessary for generating a discharge with good confinement.

The present proposal plan is: (1) To establish the CHI design for QUEST, (2) Determine the cost of the CHI hardware installation on QUEST, (3) Submit two separate proposals to support project activities. The first proposal is to the Japanese agency for CHI hardware installation on QUEST. The second proposal is to the US agency to support activities related to the fabrication of a suitable power supply for transient CHI operation on QUEST. We have now completed activity #1 and are working on activity # 2.

Brief summary of the evolution in the CHI electrode design for QUEST:
On January 21, 2013 the version of the CHI electrode design previously worked out by Dr. Raman, Professor Jarboe and Professor Ono was discussed with Professor Hanada of the QUEST group. Based on these discussions, Professor Hanada arranged for a representative from an engineering company (Mr. Hiraku Noda of V-Tech Limited) to visit QUEST on January 23. Based on the January 21 discussions, R. Raman made a simplified presentation of the main features of the CHI design for discussions with Mr.

* We acknowledge helpful discussions with Prof. Zushi, Mr. Noda (V-Tech Limited) and Mr. Rogers (Univ. of Washington) and with other members of the QUEST Team.

Hiraku Noda. Two aspects of the design were emphasized. These are: (1) assembly of the electrodes and (2) robustness of the current feeds to the CHI electrode plates. On January 28, Mr. Noda returned back to QUEST with engineering drawings that showed the design of the CHI electrode design for QUEST. Following the discussions on January 23, during the later part of the week of January 23, an improved design of the current feed design was developed. This was discussed with Mr. Noda. During discussions between Dr. Raman, Professor Hanada and Mr. Noda (on January 28), a few more improvements were made to the details of the electrode assembly. These changes were necessary so as to find a way to assemble the electrodes in the confined space near the lower divertor region of QUEST. Mr. Noda has since then incorporated these changes and provided us with copies of the final CHI electrode design for Quest. These are now being used to establish the overall project cost.

CHI Design for Quest

Here we describe the major components of the updated CHI system design for Quest. The reference CHI electrode design for CHI consists of the following components.

- An electrode with an inner/outer radius of 43/85 cm (42 cm wide)
- The Z-location of the plasma facing side of the electrode is at -1.09 m from the machine center
- The electrode is mounted on top of a flat alumina insulator (2 cm in thickness)
- The Alumina and electrode plates are mounted on the QUEST divertor plate, which is lowered by about 13 cm. This requires reducing the height of the divertor plate support legs by 13cm.

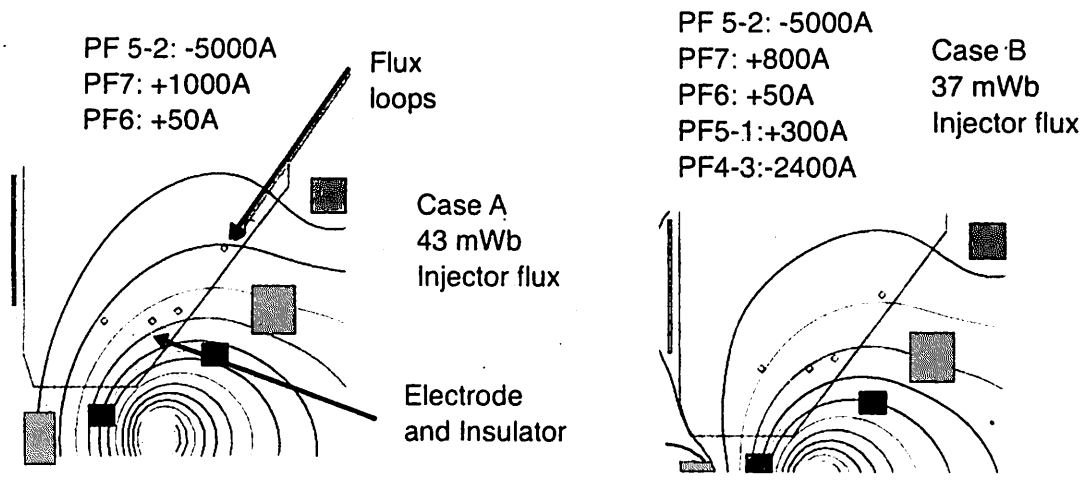

Figure 1: The flux loops for measuring the injector flux are shown by the red points and are located at (R,Z) of (0.56,-1.10) (0.77,-1.10) for the horizontal section and (0.884,-1.055) (1.090,-0.776) for the inclined section. For these calculations, to be conservative, an electrode width of 21 cm is used.

Figure 1 shows the amount of injector flux that will connect the electrode to the outer vessel. It is approximately 43mWb for the case shown on left and 37 mWb for the case shown on the right. Depending on the plasma inductance, this should result in a current generation potential of about 100-150kA during transient CHI start-up.

In Case B, other nearby coils are also used to shape the injector flux.

Figure 2 shows the layering of the electrode plate.

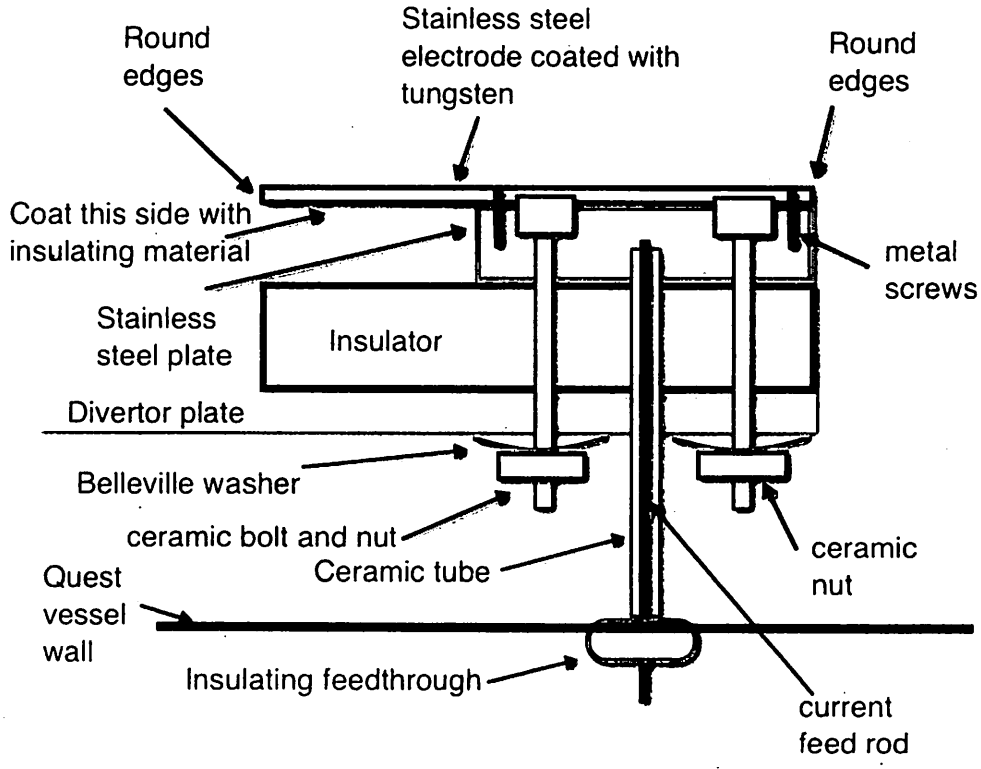

Figure 2: Qualitative sketch showing the electrode assembly details on Quest

The essential features are:

- The stainless steel electrode plate would be fabricated in the shape shown in the sketch.
    - The top and left side edges would be rounded. The larger radius edge (near the outer vessel wall) would have a rounding radius of 0.25 of the vertical thickness of the plate at the larger radius. The smaller radius edge would have a radius of 0.5 times the thickness of the plate near the smaller radius side. The plate is 1 cm thick.
- The top of the plate would be coated with high-quality dense tungsten (1 mm thick) using a state-of-the-art vacuum plasma spray process.

- This is vital for generating clean discharges. It is important to avoid contamination of the tungsten during the plasma spray process. In addition, the fabricated SS parts must be thoroughly, and ultrasonically cleaned in an oil removing solvent and baked to high temperature before sending it to the facility where it will be plasma sprayed.
- If the cost of coating is too expensive this top plate could be fabricated out of molybdenum or a 1 mm thick plate of molybdenum plate could be bonded to the top of the electrode plate.

Figure 3 shows the detailed engineering drawing of the simplified assembly shown in Figure 2.

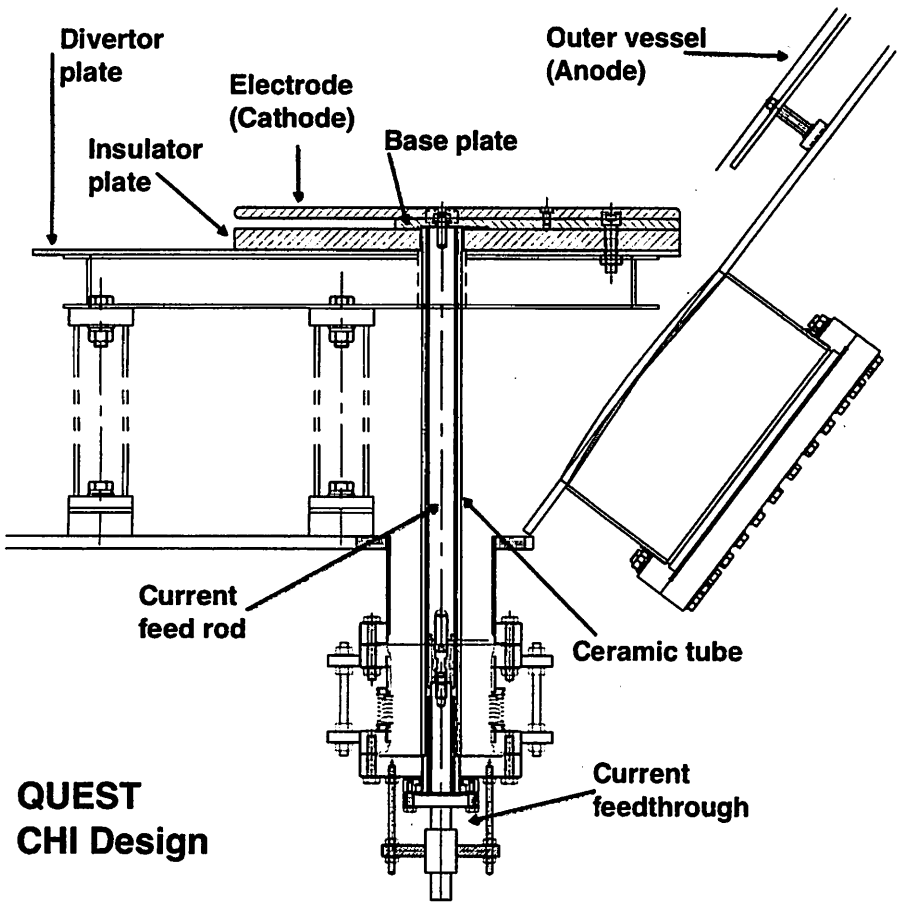

Figure 3: CHI reference design for QUEST showing (1) The insulator plate, (2) the base plate, (3) the electrode plate, (4) the current feed rod covered by a ceramic tube and (5) the current feedthrough connections to the current feed rod using a ceramic and bellows assembly.

The assembly procedure is as follows:

- The first step in the assembly process is to fasten the stainless steel base plate to the divertor plate using 10 mm diameter ceramic bolts and nuts with a suitable Belleville washer to allow for stresses during thermal expansion. The solid ceramic insulator plate is sandwiched between the SS base plate and the divertor plate.
- The current feed rod is connected to the base plate using metallic bolts. There are 2 to 3 current feed locations in the divertor area and a similar number on the outer vessel, which is maintained at ground potential, as on NSTX.
- The second step is to place the electrode plate on top of the SS base plate and connect it to the base plate using screws from the top
- The third step involves screwing the center conductor of the insulating current feed to the current feed rod using the bellows assembly. The 2.5 cm SS rod should flex less than 1 mm in 0.4 T fields when carrying a current of 5 kA. There are two to three such connections, allowing for a total current of 15 kA.

In the reference design shown in Figure 3, the following features incorporated into the design reduce the incidence of absorber arcing.

1. Use of a solid alumina insulator plate
2. A gap between the top electrode plate and the lower metal base plate that increases the tracking length when the lower part of the electrode plate extension is coated with an insulating material (plasma sprayed alumina).
3. Use of the PF5-1 coil on QUEST to shape the injector flux so that magnetic flux that originates on vessel components does not connect the upper electrode plate unless it first passes through the alumina plate.

Appendix A shows an alternate electrode assembly configuration. Some of the ideas in Appendix A could be implemented in the future if the need arises.

Appendix A: Alternate electrode arrangement

During CHI operation it is possible to create a condition know as an absorber arc. This is the region where the ExB drift is into the electrode insulating regions, instead of away from the injection region. On QUEST, this condition can occur on the smaller radius side of the electrode assembly.

We have also considered other solutions, but do not feel are necessary at this time. Parts of these solutions could be incorporated if the need arises. The changes shown below consist of the following additions to the reference design.

1) A thin metallic ring structure (shown bellow as gas shield) could be installed as small overlapping sections. This reduces the gas that is injected at the location shown in Figure A1 from entering the small radius side of the electrode assembly and thereby reduces the incidence of absorber arc.
2) The second more robust arrangement is to add an L-shaped circular section (also as smaller overlapping sections) as shown in Figure A1. The non-plasma facing side is coated with a conducting material (alumina coating). This has the advantage of significantly reducing any of the injected gas from entering the low radius side as well as it significantly increases the tracking length.

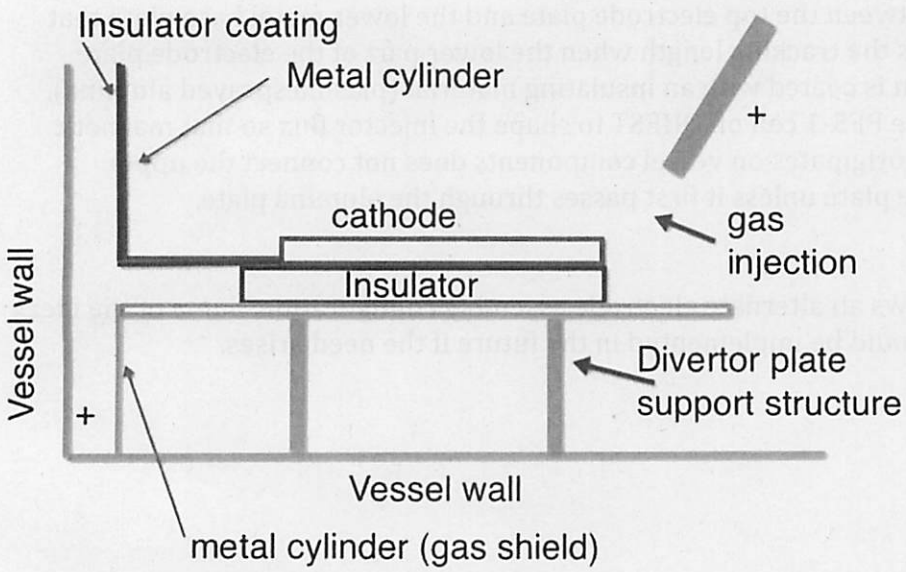

Figure A-1: The 'L' shaped cylinder structure increases the tracking length and should significantly reduce the incidence of absorber arcs. Note that some aspects of this design are included in Figure 2 through the use of an electrode with less thickness in the absorber region. The insulator-coated areas are not directly exposed to plasma.

国際化推進共同研究概要

No. 10

タイトル: A novel approach to launch EBW using a near field antenna and fast matching circuit.

研究代表者 : Wukitch, Stephan

所内世話人: 花田 和明

実施期間:

概要: 今回は先方の都合で来所はできなかったが、予定していた機器の製作は米国側で終了した。今後は低電力試験、および九大での大電力試験につなげていく予定である。ただし、米国側の装置運転に関して継続できるかどうか確定しておらず、今後については検討中である。

A novel approach to launch EBW using a near field antenna and fast matching circuit

G. Wallace, S. Shiraiwa, and S. Wukitch

MIT PSFC

Developing an efficient heating and current drive is a long-standing issue for a spherical tokamak (ST). Electron Benstein wave current drive (EBCD) is one of candidates for CD on ST. An approach to excite electrostatic EB waves in a ST plasma is to use an antenna structure designed to launch the microwave power perpendicular to the flux surface with a fast matching circuit. The maching circuit transmits the reflected microwave power back to the plasma and the space between MC layer and the launcher acts as a resonator. The eventual goal of this collaboration is to develop a new antenna based on this concept and to test it on QUEST.

A key component for this approach is a high power, electronically controlled, waveguide phase shifter. This document described the development activity carried out on PSFC. A waveguide phase shifter capable of withstanding high power (> 150 kW) for substantial pulse lengths (> 1 s) with ability to adjust phase on a fast time scale (< 1 ms) has several important applications for plasma physics experiments. The phase shifter can be used as such for control of the $k_{//}$ spectrum launched by an antenna into the plasma if multiple radiating elements are driven by the same high power source. A phase shifter is also a critical component of a feedback controlled stub tuning network, and has been deployed successfully in this capacity for impedance matching of ICRF antennas on Alcator C-Mod.

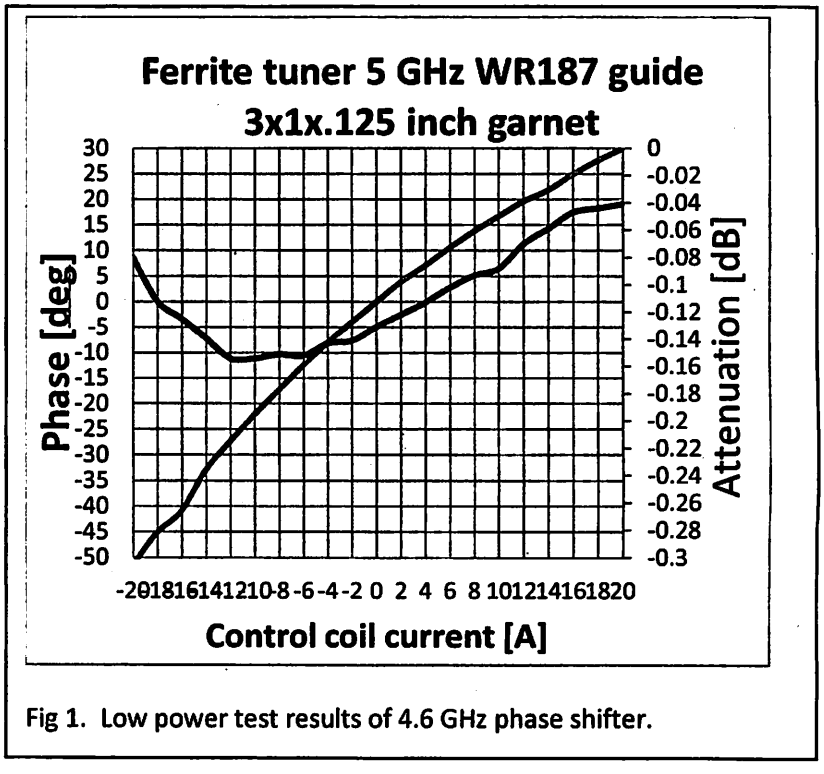

Fig 1. Low power test results of 4.6 GHz phase shifter.

The basic element of the phase shifter is a ferrite slab, in this case calcium-vanadium substituted garnet, which is positioned on the broad wall of the waveguide. The ferrite is biased by a DC magnetic field in excess of the saturation magnetization to enhance the gyrotropic properties of the ferrite. Adjustable phase shift is accomplished by offsetting the DC bias field with an

electromagnet coil. Several design iterations have resulted in a phase shifter which produces a large range of phase shift (~ 140 deg) with a reasonable amount of coil current (+/- 10 A) and low loss (S21 ~ -0.1 dB) at 4.6 GHz (see Fig 1).

The difficulty of this project lies in withstanding a high power level for significant pulse lengths. The highest power level achieved without arcing is 153 kW for 40 ms (shot 1130115532). The longest pulse (at significant power) is 415 ms at 85 kW without arcing (shot 1130115538).

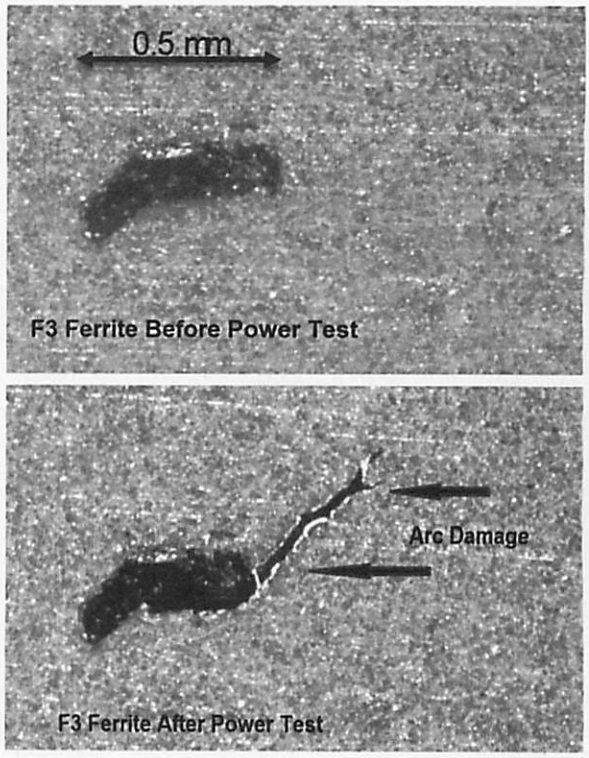

Fig 2. Micrograph of a ferrite surface void before (top) and after (bottom) arcing at high power.

Efforts to increase the maximum power and pulse length are focused on improving the ferrite material used in construction of the phase shifter. The material used in tests to date has voids on the surface around which arcs are likely to occur. Fig 2 shows a void on the surface of the ferrite before and after high power testing. Voids of 0.1-0.2 mm in size are frequent on the surface, with a maximum void size of ~ 0.5 mm. Methods for decreasing the maximum void size to < 0.1 mm were proposed by the ferrite manufacturer, which should increase power handling. Bonding of the ferrite to the waveguide wall is also under development. Tests to date have been for ferrites held in position by the DC magnetic field. Bonding of the ferrite requires first sputtering a 40 nm Ti layer onto the ferrite sample. This is followed by a 300 nm TiCu layer, then a 500 nm Cu layer is deposited on top of TiCu layer. A final 300nm of gold on top of Ti-TiCu-Cu prevents oxidation and allow for flux less soldering.

Based on the 4.6 GHz design, we tested a low power operation at 5.0 GHz. This modification required a change in the permanent magnets, but retained the same ferrite material, electromagnet coil, and waveguide design. Increasing the frequency to 8.5 GHz would require more substantial modifications including a change from WR187 to WR112/WR90, smaller ferrite slabs, and new electromagnet coils.

[Reference]

G. Wallace, S. Shiraiwa, J. Hillairet, et. al., *"Advances in lower hybrid current drive technology on Alcator C-Mod"*, presented at FEC2012, submiited to Nucl. Fusion

G. Wallace, et. al, *"Development of an electronically controlled, high power, waveguide phase shifter and stub tuner for lower hybrid current drive"*, presented at KSTAR conference 2012